

1 Translational initiation in *E. coli* occurs at the correct sites genome-wide in the absence of mRNA-rRNA  
2 base-pairing

3  
4  
5  
6 Kazuki Saito<sup>1</sup>, Rachel Green<sup>1,2</sup>, Allen R. Buskirk<sup>1\*</sup>

7  
8  
9  
10 <sup>1</sup>Department of Molecular Biology & Genetics, <sup>2</sup>Howard Hughes Medical Institute, Johns Hopkins  
11 University School of Medicine, Baltimore, MD 21205

12  
13  
14  
15 \*To whom correspondence should be addressed, [buskirk@jhmi.edu](mailto:buskirk@jhmi.edu)  
16

17 **Abstract**

18

19 Shine-Dalgarno (SD) motifs are thought to play an important role in translational initiation in bacteria.  
20 Paradoxically, ribosome profiling studies in *E. coli* show no correlation between the strength of an  
21 mRNA's SD motif and how efficiently it is translated. Performing profiling on ribosomes with altered  
22 anti-Shine-Dalgarno sequences, we reveal a genome-wide correlation between SD strength and  
23 ribosome occupancy that was previously masked by other contributing factors. Using the antibiotic  
24 retapamulin to trap initiation complexes at start codons, we find that the mutant ribosomes select  
25 start sites correctly, arguing that start sites are hard-wired for initiation through the action of other  
26 mRNA features. We show that A-rich sequences upstream of start codons promote initiation. Taken  
27 together, our genome-wide study reveals that SD motifs are not necessary for ribosomes to determine  
28 where initiation occurs, though they do affect how efficiently initiation occurs.

29

30 **Keywords:** Shine-Dalgarno, ribosome profiling, retapamulin, translational initiation

31

32

33

34

35



## 36 **Introduction**

37

38 Translational initiation is a critical step in the regulation of gene expression that impacts which proteins  
39 are synthesized and to what extent. Unlike eukaryotic ribosomes, which scan from the 5'-end of  
40 messages and generally initiate at the first start codon, bacterial ribosomes can initiate at any position  
41 along an mRNA; this is a critical requirement because many bacterial mRNAs are polycistronic.

42 Bacterial ribosomes must select the correct start codons amidst a vast excess of potential sites (AUG,  
43 GUG, and to some extent UUG) that have to be ignored. Not only does initiation determine where  
44 translation occurs (and therefore which proteins are made), in most cases the rate of initiation  
45 determines the level of protein output. In bacteria, a common strategy for regulating translation is to  
46 block ribosome recruitment to an mRNA through the action of small RNAs (Altuvia et al., 1998;  
47 Majdalani et al., 1998; Storz et al., 2004), small-molecule binding riboswitches (Winkler et al., 2002;  
48 Mandal and Breaker, 2004), and regulatory proteins (Moine et al., 1990; Babitzke et al., 2009).

49

50 Initiation rates vary in response to several mRNA features that determine how effectively an mRNA  
51 recruits 30S subunits to the start codon. Thermodynamically stable secondary structures surrounding  
52 the initiation site prevent 30S recruitment (Hall et al., 1982; de Smit and van Duin, 1990). The kinetics  
53 of RNA folding and unfolding are also critical (de Smit and van Duin, 2003; Espah Borujeni and Salis,  
54 2016): some structures exist in an unfolded state for such a short period of time that 30S subunits  
55 cannot find the start codon quickly enough by diffusion alone. In several well-characterized examples,  
56 regions of single-stranded RNA known as standby-sites are found nearby, positioning 30S subunits in  
57 close proximity so that they can efficiently capture the start codon upon unfolding of the mRNA  
58 secondary structure (de Smit and van Duin, 2003; Espah Borujeni et al., 2014). Interactions of 30S  
59 subunits and single-stranded mRNA regions (especially those that are AU-rich) can be mediated  
60 through ribosome protein S1 (Boni et al., 1991; Komarova et al., 2005). Bound on the back of the 30S  
61 subunit, the S1 protein contains multiple RNA-binding domains that can recruit mRNA and melt  
62 secondary structures (Qu et al., 2012), facilitating hybridization of 16S rRNA with complementary  
63 mRNA sequences colloquially known as Shine-Dalgarno motifs.

64

65 Shine-Dalgarno motifs have the consensus sequence GGAGG and can base pair with as many as 9 nt in  
66 the 3' terminal sequence of 16S rRNA (ACCUCCUUA in *E. coli*) referred to as the anti-Shine Dalgarno or  
67 ASD (Shine and Dalgarno, 1974). Pairing of the SD-ASD sequences can recruit 30S subunits to the start  
68 codon 5-10 nt downstream (Steitz and Jakes, 1975). SD motifs that differ significantly from the  
69 consensus or that are positioned too close or too far from the start codon yield lower levels of  
70 initiation. Indeed, many experiments using reporter genes showed that raising the SD-ASD affinity  
71 increases protein output, demonstrating its importance for determining translation levels (Hui and de  
72 Boer, 1987; Jacob et al., 1987; de Smit and van Duin, 1990; Salis et al., 2009). In addition, the SD model  
73 serves as the foundation of practical bioengineering efforts ranging from optimizing expression of  
74 recombinant proteins to expansion of the genetic code (Rackham and Chin, 2005; Salis et al., 2009).

75  
76 On the other hand, even though the ASD in 16S rRNA is almost universally conserved throughout the  
77 bacterial kingdom (Nakagawa et al., 2010), the percentage of genes with SD motifs varies widely  
78 between species. While well-characterized model species such as *E. coli* and *B. subtilis* have a high  
79 percentage of genes with SD motifs (54% and 78% respectively), there is little to no enrichment of SD  
80 motifs upstream of start codons in Bacteroidetes and Cyanobacteria (Nakagawa et al., 2010). In  
81 addition, although the majority of species in the phyla Firmicutes, Actinobacteria, and Proteobacteria  
82 have high percentages of SD-containing genes, several species have low percentages, arguing that the  
83 loss of this mechanism has occurred multiple times during evolution (Nakagawa et al., 2010;  
84 Hockenberry et al., 2017). These variations across the bacterial kingdom, despite the high conservation  
85 of the ASD element on the ribosome, raise questions as to how important the SD mechanism is for  
86 ribosome recruitment.

87  
88 Ribosome profiling is a method for deep sequencing of ribosome-protected mRNA fragments that  
89 allows us to define the position and number of ribosomes bound across the transcriptome at  
90 nucleotide resolution (Ingolia et al., 2009). This information allows us to calculate the ribosome density  
91 on each mRNA as a proxy for the efficiency of translation initiation. In pioneering ribosome profiling  
92 studies in bacteria, the paradoxical observation was made that there is little or no correlation between  
93 the ribosome occupancy of a gene and the strength of its SD motif (calculated using thermodynamic

algorithms for RNA pairing), as had been anticipated based on the SD model (Li et al., 2014; Schrader et al., 2014; Li, 2015; Campo et al., 2015). This surprising observation suggested that other mRNA features could effectively mask the effects of the SD correlation at the genome-wide level.

To isolate the effects of SD motifs on the global translational landscape, we expressed 16S rRNA mutants with altered (non-functional) ASD sequences, purified mutant ribosomes, and used ribosome profiling to ask how efficiently they translate each mRNA in the cell. Unlike previous studies that vary the SD motif and other mRNA-specific features, this approach allows us to specifically eliminate the SD-ASD interaction while keeping mRNA sequences and structures intact, so that we can specifically ask questions about the role the SD-ASD interaction plays in determining mRNA translation rates. Through this analysis, we observe for the first time the effects of SD motifs at the global level, revealing a linear correlation between SD strength and ribosome occupancy. We then combined our new profiling approach with retapamulin treatment to trap ribosomes at start codons (Meydan et al., 2019; Weaver et al., 2019) in order to study the role of SD motifs in selecting start codons. To our surprise, the ASD-mutant ribosomes selectively recognize the correct initiation sites as well as wild-type ribosomes, arguing that these sites are hard-wired for initiation independent of their SD-ASD pairing strength. We show that A-rich sequences recently identified by Fredrick and co-workers (Baez et al., 2019) are enriched at annotated start sites compared to other AUG codons in the transcriptome where initiation does not take place; these A-rich sequences are also found upstream of start codons in a wide variety of species across the bacterial kingdom. In addition, mRNA structure at annotated start sites is lower than at other AUG codons, facilitating 30S binding. Together, these studies refine our understanding of the role of SD motifs and other mRNA features in defining the proteomes of bacteria.

## Results

### *Selective profiling of ribosomes with mutant ASD sequences*

Studies of the role of SD motifs in promoting translation in their native contexts have been complicated by the fact that changing the sequence of an mRNA also affects other determinants of translational

regulation such as its overall structure. To perturb the function of SD motifs at the global level, we developed a new approach in which we mutate the ASD in 16S rRNA, purify the mutant ribosomes, and use ribosome profiling to ask how efficiently they translate each mRNA in the cell. This strategy provides us with a genome-wide view of the function of SD motifs in interactions with the unaltered transcriptome—all of the features of an mRNA that affects its translation are maintained, thereby isolating the effects of the SD motif mutation. In this manner, we eliminate the SD-ASD interaction as a contribution to mRNA translation rates and see how translation changes across the transcriptome.

We created three 16S rRNA alleles in which the ASD is mutated (Figure 1A). Two of these mutants were described previously in the literature. The ASD in *specialized* (S) ribosomes was inverted from CCUCC to GGAGG in a pioneering study by de Boer who showed that although these S-ribosomes were relatively inactive on endogenous transcripts, they efficiently translate a reporter gene with a complementary SD motif (Hui and de Boer, 1987). In later studies, Cunningham and Chin used genetic selections to characterize additional SD-ASD pairs and improve their selectivity, creating *orthogonal* (O) ribosomes where the ASD is mutated to UGGGA (Lee et al., 1996; Rackham and Chin, 2005). Ribosomes with mutant ASD motifs (like S and O) have been used in numerous studies of protein synthesis where they selectively translate reporter genes with complementary SD motifs (Rex et al., 1994; Neumann et al., 2010; Orelle et al., 2015). In addition to these two ASD mutants, we constructed a third (A) with the ASD sequence AAAAA that we anticipated would bind mRNA more weakly than the O- or S-ribosomes (given that their ASD sequences are G-rich). The MS2 aptamer was inserted into these three ASD mutants to facilitate their purification as described below (Youngman et al., 2004; Youngman and Green, 2005); as a control, we also created an MS2-tagged 16S rRNA with the canonical ASD sequence (C).

These four 16S rRNA mutants were expressed from plasmids in *E. coli* MG1655 containing the normal complement of seven wild-type rRNA operons to sustain growth. Because overexpression of ASD mutants is toxic (Jacob et al., 1987), we induced expression for only 20-25 min during which growth rates were not affected (Figure 1-figure supplement 1A). Polysome profiles from the four mutants were similar (Figure 1-figure supplement 1B) suggesting that translation remains robust during the

transient expression of MS2-tagged 16S mutants whether the ASD is intact (C) or mutated (S, O, and A). A previous study of orthogonal ribosomes suggested that altering the ASD in 16S rRNA reduces rRNA processing efficiency, leading to the accumulation of processing intermediates, but that mature rRNAs containing ASD mutations have the correct 3'-end (Aleksashin et al., 2019). To look for processing defects in our system, we performed RNA-seq on affinity-captured MS2-tagged rRNA without nuclease digestion. As shown in Figure 1-figure supplement 1C, we do not observe the accumulation of precursors with 3'-extensions or other defects in the processing of the 3'-end of 16S rRNA. This result indicates that correctly processed rRNA is produced and should be able to form mature 30S subunits.

RT-PCR with primers that distinguish endogenous 16S rRNA from the MS2-tagged mutants was used to ask whether the ASD mutants are found in actively translating polysomes (Figure 1-figure supplement 1D). We observed that the signal from C-ribosomes is equally strong in the lysate, light, and heavy polysome fractions. In contrast, the signal from the three ASD mutants is present but weaker in the polysome fractions than in the lysate. These data show that although ribosomes with mutant ASDs can engage in translation, their activity is impaired, consistent with earlier studies. Keeping this in mind, we focus our analyses not on their absolute activity but on their selectivity, asking which mRNAs they translate better than other mRNAs.

To purify mutant ribosomes, we employed a method previously developed for in vitro biochemical studies of ribosomes with lethal mutations (Youngman et al., 2004; Youngman and Green, 2005): the MS2 aptamer was fused to helix 6 of 16S rRNA allowing us to capture mutant ribosomes through their interaction with the MS2 coat protein (Figure 1B). To avoid pulling down wild-type ribosomes bound to the same mRNA as mutant ribosomes, we first treated cell lysates with RNase T1 to collapse polysomes to monosomes prior to isolating MS2-tagged ribosomes. RT-PCR reveals how well this purification strategy works: although signal from the wild-type 16S rRNA predominates in cell lysates (lower band, Figure 1C), it is nearly undetectable in purified ribosome samples eluted from the MS2-coat protein column. These data show that MS2-tagged ribosomes can be isolated with high purity for ribosome profiling studies; we refer to this procedure as MS2RP.

Comparison of the translational landscape of the canonical (C) to the orthogonal (O)-mutant confirms that the MS2RP strategy is effective. For 2217 genes with adequate coverage in each sample, we computed ribosome occupancy (RO) values by dividing the ribosome profiling density by RNA-seq density. Although we recognize that RO is not a perfect measure of initiation rates—it may also reflect differences in elongation in some cases—the number of ribosome footprints correlates strongly with protein levels in exponentially growing *E. coli* cultures (Li et al., 2014); RO therefore reports on the level of protein output per mRNA. We observed compelling differences in RO values for many genes in the two samples (Figure 1D). An initial straightforward expectation is that genes with SD motifs with high affinity to orthogonal (O) ASD sequence would have high RO values in MS2RP data from O-ribosomes; indeed, we observe that a complementary SD motif (UCCCG) 5 nt upstream of the start codon gives the *hemA* gene 10-fold higher RO with the O-ribosome than with the C-ribosome (Figure 1E). The same phenomenon was observed on *rbsK* (7-fold higher RO) and *mreB* (10-fold higher RO) with the O-ribosome and on *sapA* (9-fold higher RO) and *rsmH* (4-fold higher RO) with the S-ribosome (Figure 1-figure supplement 2). In each of these examples, the increase in RO can be attributed to higher levels of translation because the mRNA differs by less than two-fold. These examples are quite rare, however, because endogenous genes have evolved to interact with the canonical ASD and so the probability of finding a sequence with strong complementarity to the mutant ASD at just the right position is relatively low. Indeed, our data are most consistent with the conclusion that all three ASD mutants essentially act as general loss of function mutants.

### *The global role of SD motifs on the endogenous translational landscape*

We next used MS2RP to isolate the effect of SD motifs on global translation, asking to what extent they drive translation under optimal growth conditions. For each gene, we computed the SD strength as the inverse of the free energy ( $-\Delta G$ ) of pairing between the sequence -15 to -6 nt upstream of the start codon and the wild-type ASD (ACCUCCU). Based on the well-known role of SD motifs in promoting translational initiation, the expectation is that genes with strong affinity should have high RO values, and conversely, genes with weak affinity should have low RO values, yielding a strong correlation. However, our analysis of data from canonical (C) ribosomes showed only a very weak correlation

(Figure 2A), consistent with previous reports from ribosome profiling studies (Li et al., 2014) showing that SD strength has little power to predict ribosome occupancy in *E. coli*. Strikingly, the RO values from the three ASD mutants (S, O, and A) showed a robust *negative* correlation with SD affinity for the wild-type ASD sequence (Figure 2B and Figure 2-figure supplement 1). In other words, ASD mutant ribosomes translate genes with weak SD motifs better than genes with strong SD motifs.

Because the ASD mutants are unlikely to participate in SD-ASD interactions, RO values in these samples reflect the contributions of all the other mRNA elements that promote initiation. The observation that these other elements yield a negative correlation with SD strength suggests that they in general counteract the positive correlation contributed by SD-ASD pairing (with wild-type ribosomes). As such, these contributions effectively mask the effect of SD motifs in Figure 2A. By calculating the difference in RO ( $\Delta\log\text{RO}$ ) for each gene between the C- and A-ribosomes, we effectively subtract all the mRNA elements that determine RO independent of SD-ASD pairing, thus isolating the effects of the SD motifs on mRNA translation rates. The  $\Delta\log\text{RO}$  term reflects how much better a message is translated by wild-type ribosomes than by ASD mutants. When  $\Delta\log\text{RO}$  values are plotted as a function of SD-ASD affinity ( $-\Delta G$ ) using the wild-type ASD sequence, we observe a strong linear correlation with SD-ASD affinity for each of the mutants (Figure 2C and Figure 2-figure supplement 1). As expected, genes with strong SD motifs are translated better by ribosomes with the canonical ASD than by ASD-mutant ribosomes. The fact that we observe this correlation validates our calculations of SD strength; analysis of the distance of SD motifs from the start codon confirms that genes with the highest  $\Delta\log\text{RO}$  have the strongest SD affinity in the -15 to -6 region as shown in previous studies (Figure 2-figure supplement 2). These data obtained with MS2RP reveal for the first time the effect of SD motifs on translation genome-wide, consistent with their characterized role in promoting initiation.

#### *SD motifs are not necessary for start codon selection*

SD motifs are also widely held to play a critical role in recognizing and selecting initiation sites (Steitz and Jakes, 1975). In the analyses described so far, we have used MS2RP to estimate the ribosome density on each mRNA as a proxy for initiation rates in order to address questions about *how much*

translation is occurring on annotated genes. These data are less informative about the degree to which mutant ribosomes initiate at the wrong sites in the transcriptome. Non-canonical initiation is difficult to observe in *E. coli* because 5'- and 3'-untranslated regions of mRNAs are generally quite short and translation at alternate start codons within ORFs is swamped by the signal of elongating ribosomes from the canonical start site. In eukaryotes, the antibiotics harringtonine and lactimidomycin have been used with great success together with ribosome profiling to identify sites where translational initiation takes place (Ingolia et al., 2011; Lee et al., 2012). These compounds do not interfere with elongating ribosomes, allowing them to continue translation and terminate normally. In contrast, they trap newly-initiated ribosomes, providing a way of identifying initiation sites in ribosome profiling studies. Two antibiotics were recently shown to similarly specifically trap initiation complexes in bacteria: Onc112 and retapamulin (Meydan et al., 2019; Weaver et al., 2019).

To study the role of SD motifs on start codon selection, we treated cells with retapamulin for 5 min and then used MS2RP to identify start sites occupied by ribosomes with the various ASD sequences. For example, elongating wild-type (C) ribosomes are found all across the *lpp* gene in untreated cells (Figure 3A, light grey), whereas they are highly enriched at the annotated start codon in retapamulin-treated cells (dark grey). As expected, ribosome footprints are not seen at three internal AUG codons, since these do not function as initiation sites. Strikingly, in retapamulin-treated cells, the A-ribosomes also find the correct start site, ignoring the three other AUG codons (Figure 3A, dark green). In another example, the *gmk* gene, both C- and A-ribosomes are enriched at the annotated start codon in retapamulin-treated cells but not at several internal AUG codons (Figure 3B). In both examples, both WT and mutant ribosomes select the correct, annotated start site while ignoring other AUG codons.

To analyze the accuracy of start codon selection by the ASD variants in retapamulin-treated samples genome-wide, we computed the average number of ribosome footprints across many genes aligned at their annotated start codons or aligned at all the other AUG triplets in the transcriptome (non-annotated AUGs). Our initial expectation was that in the absence of SD-ASD base pairing, the mutant ribosomes might fail to recognize the correct start sites and bind more often to other AUG triplets in the transcriptome. Strikingly, both the C- and A-ribosomes show strong initiation peaks at annotated



268 AUGs (Figure 3C), whereas these peaks are absent in both samples at non-annotated AUGs (Figure 3D).  
269 These results provide initial evidence that ribosomes correctly select annotated start sites genome-  
270 wide in the absence of the SD-ASD interaction.

271  
272 To further explore this surprising finding, we next asked how the affinity of mRNA-rRNA base pairing  
273 influences initiation at annotated start codons. We assumed that for the mutant ribosomes, base  
274 pairing would play little or no role in initiation because they would likely have low affinity for  
275 annotated start sites that evolved to bind the wild-type ASD. To test this assumption, we calculated the  
276 affinity of each mutant ASD for the sequence upstream of the start codon of each gene. We grouped  
277 genes into different sets based on these affinities and plotted the average number of ribosome  
278 footprints at the annotated start sites as in Figure 3C. In the subset of genes with no predicted affinity  
279 for any of the three ASD mutants ( $\Delta G > -1$ ), we still see robust enrichment of A, O, and S ribosomes at  
280 the annotated start sites (Figure 3E). Since all three ASD variants initiate at annotated start sites, these  
281 data argue against the possibility that serendipitous base-pairing between the mRNA and the mutant  
282 ASD sequences explains this enrichment.

283  
284 We also analyzed a set of annotated start sites with strong calculated affinity to the wild-type ASD.  
285 These sites are expected to be dependent on the SD-ASD interaction. Yet we again observed robust  
286 start peaks for each ASD variant ribosome, indicating that SD-ASD pairing is dispensable for initiation  
287 even in genes with strong SD motifs (Figure 3-figure supplement 1A). Furthermore, we found that in a  
288 set of sites with predicted high affinity to the ASD of the O-ribosome, there was strong enrichment of  
289 A- and S-ribosomes at start codons, despite the differences in the ASD sequence (Figure 3-figure  
290 supplement 1B). Likewise, in a set of genes with predicted high affinity to the ASD of the S-ribosome,  
291 there was strong enrichment of O- and A-ribosomes at start codons (Figure 3-figure supplement 1C).  
292 (There were too few genes with high affinity to the A-rich ASD sequence to perform an equivalent  
293 analysis for A-ribosomes). Taken together, these analyses show that annotated initiation sites are hard-  
294 wired for initiation independent of their potential for base pairing between the mRNA and rRNA.

295  
296 *SD motifs are not necessary for initiation at non-canonical sites*

297

298 We next asked what role mRNA-rRNA pairing plays in initiation at AUG triplets in the transcriptome  
299 that are not normally used for initiation (non-annotated AUGs). For this purpose, we used data from  
300 retapamulin-treated cells to calculate an initiation score (IS) for each AUG triplet, defined as the  
301 average number of reads mapped within 3 to 21 nt downstream of an AUG (to capture footprints of  
302 various sizes) divided by the average number of reads mapped over a wider spacing (100 nt, Figure 4A).  
303 The first and most general finding is that the  $\log_2$ IS values from the C- and A-ribosomes have a similar  
304 distribution with medians close to 0 (Figure 4B), indicating that footprints from the A-ribosomes are  
305 not enriched at non-annotated AUG codons. This result is consistent with the average gene plot shown  
306 in Figure 3D and with the fact that most of these AUG codons do not serve as initiation sites. To better  
307 characterize the difference between C- and A-ribosomes in initiation at non-annotated AUG codons,  
308 we selected a subset of sites that effectively recruit C-ribosomes and yield strong initiation peaks.  
309 These sites have  $\log_2$ IS values  $> 1.5$  and are highlighted in black in Figure 4B. Surprisingly, this same  
310 subset of AUG codons also shows high IS values for A-ribosomes (Figure 4C), arguing that SD-ASD  
311 pairing is not the feature that explains why initiation takes place at these specific AUG triplets and not  
312 at others.

313

314 To further characterize how SD-ASD pairing affects initiation at non-annotated AUG triplets, we  
315 grouped potential initiation sites by their affinity for wild-type or mutant ASDs as described above for  
316 annotated start sites. For sites with high affinity to the ASD of the S-ribosome, for example, the  
317 distribution of IS values for S-ribosomes closely resembled the other three ribosomes (Figure 4E), with  
318 median values near zero. These data show that the presence of a complementary Shine-Dalgarno-like  
319 sequence near an AUG codon is not sufficient to recruit S-ribosomes and generate a robust start codon  
320 peak. We selected the subset of AUGs with high affinity to S-ribosomes where initiation occurs with S-  
321 ribosomes ( $\log_2$ IS  $> 1.5$ , dark red in Figure 4E). As expected, these high-IS sites show strong start peaks  
322 with S-ribosomes; however, the other ribosomes with different ASD sequences show robust start  
323 peaks as well (Figure 4F). Similarly, low-IS sites that are not translated by S-ribosomes (light red in  
324 Figure 4E) are also not translated by the other ribosomes (Figure 4G). The observation that SD-ASD  
325 pairing does not contribute to initiation at these sites with high affinity to the S-ribosomes also holds

326 true for non-annotated AUGs with high affinity to the wild-type ASD (Figure 4-figure supplement 1).  
327 Once again, these data argue that AUGs that recruit ribosomes and lead to initiation are hard-wired for  
328 this purpose irrespective of the strength of the mRNA-rRNA base pairing interaction. Taken together,  
329 these data on initiating ribosomes show that mRNA-rRNA base pairing is neither necessary nor  
330 sufficient for translational initiation.

331

### 332 *A-rich sequences upstream of start codons promote initiation*

333

334 To provide insight into mRNA features other than SD strength that might contribute to ribosome  
335 recruitment, we asked which features are enriched at annotated start sites. To avoid interference from  
336 SD motifs, we selected only annotated start sites with low affinity to the wild-type ASD ( $\Delta G > 0$ ) and  
337 compared them to non-annotated AUG codons, most of which do not lead to initiation. We observed  
338 enrichment of adenosines (A) at many sites within 15 nt upstream of the start codon and 5 nt  
339 downstream (Figure 5A).

340

341 To test whether these A's promote translation, we selected four mRNAs with A-rich initiation sites (and  
342 weak SD motifs) and established a GFP reporter assay to follow their activity (Figure 5B). Of these four  
343 mRNAs (Figure 5C), two contain *annotated* initiation sites with low ASD-affinity, the start codons from  
344 *yhbY* and *gsk*. We also selected two representative *non-annotated* AUG codons found within the *creA*  
345 and *yeiR* genes; these sites have high IS values in both the C-ribosome and O-ribosome MS2RP data  
346 from retapamulin-treated cells. The sequences surrounding these four AUG codons (from 30 nt  
347 upstream to 45 nt downstream) were fused in frame to GFP such that GFP fluorescence reports on the  
348 activity of the AUG of interest. In addition to the wild-type sequence, we constructed mutants in which  
349 all of the A's 15 nucleotides upstream of AUG were changed to either U's or C's (G's were avoided  
350 because they have high affinity for the ASD). The reference protein mCherry was also expressed from  
351 the same plasmid with a standard ribosome binding site. The GFP/mCherry ratio was then normalized  
352 to a control lacking the GFP sequence (measuring only cellular auto-fluorescence).

353

354 We observed that the GFP/mCherry ratio was higher than background for all four AUG codons,

355 showing that all are capable of driving GFP expression (Figure 5D). The two annotated start sites from  
356 *yhbY* and *gsk* induced stronger GFP expression than the non-annotated start sites, *creA\** and *yeiR\**.  
357 Importantly, however, the fact that fluorescence was observed from these latter examples confirms  
358 the results from the MS2RP data from retapamulin-treated cells showing that they are translated to  
359 some extent by wild-type ribosomes. We observed that replacement of the A's with U's lowered GFP  
360 expression in all cases except for *yeiR\** which showed the weakest GFP expression. A stronger effect  
361 was observed by changing the A's to C's, which led to complete loss of GFP fluorescence from all four  
362 AUG contexts tested. These results support our hypothesis that A-rich sequences upstream of start  
363 codons contribute to the identification of translational start sites.

364

365 The ability of A-rich sequences to promote initiation is likely not limited to *E. coli*: when we compared  
366 the local context of AUG codons in annotated start sites vs. non-annotated AUG codons for a set of  
367 diverse bacteria, we again saw that A-rich sequences were enriched (Figure 5-figure supplement 1). For  
368 *E. coli* and most other species examined, the enrichment of A's was weaker than the enrichment of G's  
369 corresponding to the SD sequence, but for *Mycoplasma pneumoniae* and *Flavobacterium johnsoniae*,  
370 the SD signal is not observed and there the enrichment of A's is particularly striking. A-rich sequences  
371 are highly conserved and may serve as an important mechanism for start site selection in these  
372 species, while contributing broadly to more diverse species.

373

374 *mRNA structure is lower at annotated start sites than at non-annotated AUG codons*

375

376 In bacteria, mRNA structure surrounding the start codon has been shown in mechanistic studies to  
377 reduce ribosomal occupancy (Lodish, 1970; de Smit and van Duin, 1990; de Smit and van Duin, 2003;  
378 Espah Borujeni and Salis, 2016). Moreover, several transcriptome-wide analyses of mRNA structure in *E.*  
379 *coli* show lower levels of structure surrounding initiation sites (Campo et al., 2015; Burkhardt et al.,  
380 2017). We asked how mRNA structure differs between annotated start sites and internal AUG codons  
381 that are not annotated as start sites. We used data from a recent study of the structure of mRNAs in vivo  
382 using SHAPE and deep sequencing (Mustoe et al., 2018). From transcripts with sufficient coverage, we  
383 calculated the median SHAPE reactivity over a 120 nt window surrounding 365 annotated start sites and

compared it to 7,310 non-annotated AUGs (Figure 5E). For annotated initiation sites, the level of mRNA structure is significantly lower for a region 30 nt in length on both sides of the AUG codon (shown in red) as previously reported (Campo et al., 2015; Burkhardt et al., 2017). In contrast, except for a sharp dip in reactivity at the aligned AUG codon due to sequence bias, we see that mRNA structure is consistently high across this window for the set of non-annotated AUGs (shown in blue). These differences may be due in part to the ability of ribosomes to melt RNA structure during translation; indeed, initiation leads to the unfolding of RNA, which facilitates initiation by another 30S subunit (Espah Borujeni and Salis, 2016; Andreeva et al., 2018). But, given that SHAPE and DMS reactivity of mRNAs in vivo and in vitro are strongly correlated (Burkhardt et al., 2017; Mustoe et al., 2018), it is also likely that mRNA structure plays a causal role in setting initiation rates.

## Discussion

In this study, we performed ribosome profiling on mutant ribosomes purified using an RNA tag, the MS2 aptamer, a strategy we call MS2RP (Figure 1). Originally developed for in vitro studies of ribosomes containing lethal rRNA mutations (Youngman et al., 2004; Youngman and Green, 2005), MS2-tagged ribosomes also have potential to yield insights into the function of key rRNA sequences in vivo. In addition to the studies of the ASD sequence in 16S rRNA reported here, MS2RP could be employed to characterize the functions of rRNA domains on initiation, elongation, termination, and recycling at a genome-wide level in vivo. Because MS2RP can be performed on rRNA mutants expressed from plasmids, the method can be easily transferred to other bacteria or to eukaryotes without altering rDNA in the genome. Of particular interest are rRNA variants in bacterial genomes that are expressed differentially in response to changes in the environment and are proposed to have different specificities or functions (Kurylo et al., 2018; Song et al., 2019). Variant rRNA alleles have also been reported for eukaryotic cells (Parks et al., 2018); for example, different small subunit rRNA alleles are expressed in various developmental stages in *Plasmodium* (Gunderson et al., 1987). In addition, the functions of the highly variable rRNA expansion segments in eukaryotes are poorly understood (Spahn et al., 2001; Anger et al., 2013). MS2RP could be a powerful tool to elucidate the activities of various subpopulations of variant or mutated rRNAs.

413

414 Previous genome-wide studies in bacteria have shown little or no correlation between SD strength and  
415 ribosome occupancy (Li et al., 2014; Schrader et al., 2014; Campo et al., 2015). Using MS2RP, we are  
416 able for the first time to reveal the role of SD motifs in promoting initiation across the transcriptome.  
417 In our approach, we mutated the ASD on the ribosomes, thus maintaining mRNA sequence and  
418 structure, thus allowing us to isolate the effects of the SD:ASD interaction on translation. In the  
419 absence of SD:ASD pairing, we observed a strong negative correlation between ribosome occupancy  
420 and the SD strength (calculated by pairing with the wild-type ASD sequence). In other words, the  
421 mutant ribosomes translate genes with strong SD motifs worse than those with weak SD motifs (Figure  
422 2B). There are two possible explanations for this negative correlation. It may be that the binding of  
423 wild-type ribosomes to mRNAs with strong SD motifs occludes their ribosome-binding sites, preventing  
424 mutant ribosomes from initiating and efficiently translating these genes. Alternatively, mRNA structure  
425 and other features may outweigh the impact of SD motifs, masking their effects, explaining why  
426 conventional ribosome profiling studies failed to observe correlations between SD strength and  
427 ribosome occupancy. Regardless of which of these explanations is correct, the MS2RP strategy allows  
428 us to subtract the cumulative contribution to ribosome occupancy of all of such other mRNA features,  
429 and thus to focus exclusively on the contribution to ribosome occupancy of the SD:ASD interaction  
430 genome-wide. In this analysis, we are now able to see a linear correlation between the SD strength of  
431 an mRNA and protein output (Figure 2C).

432

433 Given that the SD motif functions through a well-defined mechanism and is widely conserved  
434 throughout bacteria, it has been thought to provide an important mechanism for start codon selection  
435 and translational output. Consistent with such a view, SD motifs are underrepresented within ORFs in  
436 order to avoid spurious initiation at internal start codons (Hockenberry et al., 2018). Strikingly,  
437 however, we find that ribosomes with altered ASDs still find the correct start codons about as  
438 efficiently as wild-type ribosomes (Figure 3). Start peaks for all four ribosome types are observed at  
439 annotated start sites regardless of the affinity of the ribosome binding site for the ASD. This shows that  
440 initiation sites are hard-wired for initiation based on mRNA features separate from the potential for  
441 SD-ASD pairing. These observations also hold true at the occasional non-annotated AUG codons where

442 some initiation occurs (Figure 4). These data are consistent with the conclusion that SD motifs are not  
443 essential for determining where translation starts on mRNAs genome-wide.

444  
445 What, then, are other mechanisms that could be used for start codon selection? Local mRNA structure  
446 and RNA folding kinetics clearly must play a critical role in allowing ribosomes to find the start codon. A  
447 number of mechanistic studies have demonstrated that RNA structure around the start codon lowers  
448 translation levels (Hall et al., 1982; de Smit and van Duin, 1990; Osterman et al., 2013; Espah Borujeni  
449 et al., 2014). Studies of factors that alter the expression of simplified reporter genes (involving  
450 randomization of the 5'-UTR or coding sequences) show that lack of secondary structure surrounding  
451 the initiation site has the most significant correlation with protein output (Salis et al., 2009; Kudla et  
452 al., 2009; Goodman et al., 2013). Recent transcriptome-wide analyses of mRNA structure in *E. coli*  
453 confirm that annotated start sites have lower levels of mRNA structure, as seen by PARS on purified  
454 mRNA and DMS-seq in vivo (Campo et al., 2015; Burkhardt et al., 2017). mRNA structure is likely an  
455 important factor in start site selection: using high-resolution SHAPE-MaPseq data (Mustoe et al., 2018),  
456 we showed that annotated AUGs have lower levels of RNA structure 30 nt upstream and downstream  
457 whereas internal AUG are not surrounded by regions of lower structure (Figure 5E).

458  
459 Interestingly, in comparing the sequence context of AUG codons that are annotated as initiation sites  
460 with those that are not, we found that A's are enriched both upstream and downstream of annotated  
461 initiation sites (Figure 5A) and we confirmed their importance in reporter assays (Figures 5B-D). These  
462 results from endogenous initiation sites are reminiscent of observations of the over-representation of  
463 A's in 5'-UTR sequences selected for strong affinity to the ribosome in vitro (Gao et al., 2016) and in 5'-  
464 UTRs selected from random sequences upstream of a reporter gene for high levels of translation in  
465 vivo (Evfratov et al., 2017). Comparison of annotated start sites and non-annotated AUGs across  
466 several bacterial genomes shows that this mechanism is widespread (Figure 5-figure supplement 1).  
467 Although enrichment of A's is more subtle than enrichment of G's in *E. coli* and *B. subtilis*, in organisms  
468 that lack SD motifs, such as *Mycoplasma pneumoniae* and *Flavobacterium johnsoniae*, A-rich motifs  
469 may play an important role in initiation. Indeed, in a recent study, Fredrick and co-workers used  
470 ribosome profiling in *F. johnsoniae* and observed enrichment of A's upstream of start codons in mRNAs

471 with high ribosome occupancy in comparison to genes with are translated less efficiently (Baez et al.,  
472 2019). We envision that this sequence, like the Shine-Dalgarno motif, acts as a translational enhancer,  
473 fine-tuning the efficiency of initiation.

474  
475 The mechanism by which A-rich sequences enhance initiation is not clear. The prevalence of A's may  
476 alter the mRNA dynamics; A-rich sequences tend to have less secondary structure than GC-rich  
477 sequences. We note however that replacing A's with U's in several reporters reduced translation levels  
478 even though the U's are similarly not expected to yield strong structures. A second possibility is that  
479 ribosomal components may interact specifically with A's close to the start codon that are bound inside  
480 the ribosome during initiation. Fredrick and co-workers used reporter assays to show that mutation of  
481 a particular A at the -3 position reduces expression; this result is intriguing because the classic Kozak  
482 sequence (GCC(A/G)CCAUG) that promotes high levels of translation in eukaryotes also contains a  
483 purine at position -3. A-rich sequences have been reported to enhance translation in a variety of  
484 eukaryotic contexts including *Drosophila* and wheat germ and reticulocyte lysates (Ranjan and Hasnain,  
485 1995; Sano et al., 2002; Suzuki et al., 2006; Pfeiffer et al., 2012). It may be that A-rich sequences  
486 interact with conserved elements of the ribosome across the domains of life. A's further from the start  
487 codon (10-20 nt upstream) may interact with bacteria-specific ribosomal protein S1. bS1 preferably  
488 binds to A/U-rich sequence elements upstream of SD sequences (Boni et al., 1991; Komarova et al.,  
489 2005) and is thought to unwind mRNA structure to induce initiation (Qu et al., 2012; Duval et al., 2013).

490  
491 Our findings have broad implications for the evolution of translational mechanisms in bacteria. Not all  
492 bacteria utilize SD motifs to promote translational initiation—SD motifs are notably lacking in  
493 Bacteroidetes and Cyanobacteria. Because the prevalence of SD motifs is a feature of the genome in  
494 general and not of a single gene, it makes sense that evolutionary selective pressure for or against SD  
495 usage would act at the level of the transcriptome. The nature of these selective pressures remains  
496 unclear, although Hockenberry recently argued that bacteria with high levels of SD usage tend to have  
497 higher maximal growth rates (Hockenberry et al., 2017). Future studies will clarify the evolutionary  
498 relationship between the growth environment, levels of SD usage among bacterial species, and their  
499 transcriptome-wide effects.



500  
501  
502  
503  
504  
505  
506  
507  
508  
509  
510  
511  
512  
513  
514  
515  
516  
517  
518  
519  
520  
521  
522  
523  
524  
525  
526  
527  
528  
529

**Acknowledgments**

The authors thank Daniel Goldman, Colin Wu, and Boris Zinshteyn for critical reading of the manuscript, as well as David Mohr at the Genetics Resources Core Facility, Johns Hopkins Institute of Genetic Medicine, for sequencing assistance. This study was funded by a JSPS fellowship (K.S.), NIH grant GM110113 (A.R.B.), and HHMI (R.G.).

**Declaration of Interests**

The authors declare no competing interests.

**Data availability**

The sequencing data are available in processed WIG format at the GEO using accession number GSE135906 and as the raw FASTQ files at the SRA. Custom python scripts used to analyze the sequencing data are freely available at [https://github.com/greenlabjhmi/2019\\_SDASD](https://github.com/greenlabjhmi/2019_SDASD).

**Materials & Methods**

*Growth conditions*

Unless otherwise specified, cells were cultured at 37 °C in 500 mL of LB + ampicillin (50 mg/L). IPTG was added (0.3 mM final) when the culture reached OD<sub>600</sub> = 0.3 and cells were harvested by filtration at OD<sub>600</sub> = 0.5. For profiling with retapamulin, cells were grown at 37 °C in 500 mL of LB + ampicillin to OD<sub>600</sub> = 0.3, induced with IPTG, grown to OD<sub>600</sub> = 0.45, and then harvested by filtration 5 min after the addition of retapamulin (100 µg/mL final).

*Cell harvest and lysis*

Cells were harvested by filtration using a Kontes 99 mm filtration apparatus and 0.45 µm nitrocellulose filter (Whatman) and then flash frozen in liquid nitrogen. Cells were lysed in lysis buffer (20 mM Tris pH 8.0, 10 mM MgCl<sub>2</sub>, 100 mM NH<sub>4</sub>Cl, 5 mM CaCl<sub>2</sub>, 100 U/mL DNase I, and 1 mM chloramphenicol) using a Spex 6870 freezer mill with 5 cycles of 1 min grinding at 5 Hz and 1 min cooling. Lysates were centrifuged at 20,000 g for 30 min at 4 °C to pellet cell debris.

530 *Overexpression and purification of MBP-MS2-His protein*

531 BL21(DE3) cells were transformed with the plasmid pMal-c2G-MBP-MS2-His, cultured at 37 °C in LB +  
532 ampicillin (50 mg/L) to OD<sub>600</sub> = 0.7, and induced with 0.3 mM final IPTG for 4 h at 37 °C. Cells were  
533 harvested by centrifugation and lysed on a french press in the binding buffer (50 mM NaH<sub>2</sub>PO<sub>4</sub> pH 8.0,  
534 300 mM NaCl, 10 mM imidazole, 6 mM BME). The MBP-MS2 protein was purified by FPLC (Atka, GE);  
535 after washes with the binding buffer, it was elution with the binding buffer supplemented with 200  
536 mM imidazole.

537

538 *Affinity purification of MS2-tagged ribosomes*

539 3 mL of amylose resin (NEB) were transferred to a Poly-Prep Chromatography Column (Bio-Rad) and  
540 washed 3 times with 10 mL of lysis buffer. 2.5 mg of MBP-MS2-His protein were loaded onto the  
541 amylose resin, incubated at 4 °C for 1 h, and washed twice with 10 mL of lysis buffer. For MS2RP, 1.5  
542 mL of cell lysate and 15 µL of RNase T1 (1000 U/µL, Thermo) were loaded onto the MBP-MS2 resin,  
543 incubated at 4 °C for 2 h, and washed 3 times with 10 mL of lysis buffer. The resin was re-suspended in  
544 1 mL of lysis buffer and 360 µg MNase was added to digest mRNA and remove the MS2 hairpin in  
545 rRNA, releasing the ribosomes from the column. Following a 2 h incubation at 25 °C, the flow-through  
546 was collected. Another 2 mL of lysis buffer was passed through the resin and collected. The flow-  
547 through fractions were then combined.

548

549 *Sucrose density gradient centrifugation*

550 10-54% sucrose density gradients were prepared using the Gradient Master 108 (Biocomp) in the  
551 gradient buffer (20 mM Tris pH 8.0, 10 mM MgCl<sub>2</sub>, 100 mM NH<sub>4</sub>Cl, 2 mM DTT). 5-20 AU of *E. coli* lysate  
552 was loaded on top of sucrose gradient and centrifuged in a SW41 rotor at 35,000 rpm for 2.5 h at 4 °C.  
553 Fractionation was performed on a Piston Gradient Fractionator (Biocomp).

554

555 *Library preparation*

556 Libraries for MS2RP and standard ribosome profiling are prepared as in (Woolstenhulme et al., 2015;  
557 Mohammad et al., 2016). At least two biological replicates were performed for each MS2RP library as  
558 detailed in the GEO database entry. RNA-seq libraries were prepared with TruSeq Stranded Total RNA

559 Gold from 250 ng of total RNA following depletion of rRNA by RiboZero rRNA Removal Kit for bacteria  
560 (Illumina). Libraries were analyzed by BioAnalyzer high sensitivity DNA kit (Agilent) then sequenced on  
561 the HiSeq2500 (Illumina).

562

#### 563 *Analysis of rRNA purity by RT-PCR*

564 RNA was purified by hot-phenol extraction. The first strand synthesis was performed with 500 ng of  
565 total RNA, primer MS2check\_R (5'-AGACATTACTCACCCGTCCGCGCACTC-3') and SuperScript III  
566 (Invitrogen). 15 cycles of PCR amplification were performed with primer MS2check\_F70 (5'-  
567 TGCAAGTCGAACGGTAACAGGAAG-3'), primer MS2check\_R, and Phusion polymerase (NEB). PCR  
568 products were resolved by 8% TEB gel and analyzed by Typhoon FLA 9500 (GE).

569

#### 570 *GFP/mCherry assay*

571 MG1655 cells carrying the reporter plasmid were cultured in LB + ampicillin (50 mg/L) to early log  
572 phase. Cells were diluted 50-fold in TBS. GFP and mCherry fluorescence were measured on a Guava  
573 easyCyte flow cytometer (Millipore Sigma).

574

#### 575 *General processing of sequencing data*

576 For libraries prepared by linker with UMI (rAppNNNNNNCACTCGGGCACCAAGGAC), perfectly matching  
577 reads (including 5'-end and 3'-end UMI) were converted to a single read by Tally (Davis et al., 2013). 3'-  
578 linker sequences were removed by Skewer (Jiang et al., 2014). The 5' end UMI added by the RT primer  
579 were removed by seqtk. Reads were aligned using bowtie version 1.1.2 (Langmead et al., 2009), first to  
580 the tRNAs, rRNAs, and the *ssrA*, *ssrS*, *lacI* and *ffs* genes. Reads that failed to align to those sequences  
581 were aligned to *E. coli* MG1655 NC\_000913.2. Ribosome position was assigned by the 3'-end of aligned  
582 reads. RNA-seq data were assigned by the 5'-end of aligned reads.

583

#### 584 *Calculation of $\Delta G$*

585 The affinity ( $\Delta G$ ) of the ASD and the sequence of a start codon was calculated for each mRNA using  
586 free\_scan with "-l 0 -b 0" option to disallow internal loop and internal bulge (Nakagawa et al., 2010).  
587 The input sequences were -15 and -6 nt upstream of AUG and the reverse sequence of wild-type ASD

588 (UCCUCCA) or the mutant ASD where appropriate.

589

#### 590 *Analyses of genome-wide mRNA structural data*

591 Average SHAPE reactivity was based on the SHAPE-MaP data (Mustoe et al., 2018). A median of the  
592 SHAPE reactivity from the region -25 to +25 upstream and downstream of the start codon was used as  
593 degree on RNA structure.

594

#### 595 *Analyses of initiation peaks in samples treated with retapamulin*

596 AUG codons were only included in the analysis of average ribosome density and initiation scores if they  
597 had more than 10 mapped reads in the window of -50 upstream and +50 downstream of the AUG. To  
598 calculate average ribosome density, for each AUG we took the rpm at each position across this  
599 window, divided it by the total rpm in the window, and then computed the mean of these values for all  
600 AUGs included in the calculation. Initiation scores were computed by taking the mean of reads mapped  
601 within +3 to +21 nt downstream of the A in AUG and dividing it by the mean of reads mapped on the  
602 region -50 to +50 of the AUG.

603

#### 604 *Probability logo*

605 Probability logos were generated by kpLogo (Wu and Bartel, 2017) using its default settings. For Figure  
606 7A and B, input and background sequences are described in the figure legend. For Figure 4-figure  
607 supplement 1, the set of input sequences consisted of annotated AUGs from the GFF file available at  
608 NCBI and the set of background sequences consisted of all AUGs in the genome that were not  
609 annotated as initiation sites.

610

611

## REFERENCES

- Aleksashin NA, Leppik M, Hockenberry AJ, Klepacki D, Vázquez-Laslop N, Jewett MC, Remme J, Mankin AS. 2019. Assembly and functionality of the ribosome with tethered subunits. *Nat Commun* **10**:1–13. doi:10.1038/s41467-019-08892-w
- Altuvia S, Zhang A, Argaman L, Tiwari A, Storz G. 1998. The Escherichia coli OxyS regulatory RNA represses fhlA translation by blocking ribosome binding. *EMBO J* **17**:6069–6075. doi:10.1093/emboj/17.20.6069
- Andreeva I, Belardinelli R, Rodnina MV. 2018. Translation initiation in bacterial polysomes through ribosome loading on a standby site on a highly translated mRNA. *Proc Natl Acad Sci* **115**:4411–4416. doi:10.1073/pnas.1718029115
- Anger AM, Armache J-P, Berninghausen O, Habeck M, Subklewe M, Wilson DN, Beckmann R. 2013. Structures of the human and Drosophila 80S ribosome. *Nature* **497**:80–85. doi:10.1038/nature12104
- Babitzke P, Baker CS, Romeo T. 2009. Regulation of Translation Initiation by RNA Binding Proteins. *Annu Rev Microbiol* **63**:27–44. doi:10.1146/annurev.micro.091208.073514
- Baez WD, Roy B, McNutt ZA, Shatoff EA, Chen S, Bundschuh R, Fredrick K. 2019. Global analysis of protein synthesis in Flavobacterium johnsoniae reveals the use of Kozak-like sequences in diverse bacteria. *Nucleic Acids Res* **47**:10477–10488. doi:10.1093/nar/gkz855
- Boni IV, Isaeva DM, Musychenko ML, Tzareva NV. 1991. Ribosome-messenger recognition: mRNA target sites for ribosomal protein S1. *Nucleic Acids Res* **19**:155–162.
- Burkhardt DH, Rouskin S, Zhang Y, Li G-W, Weissman JS, Gross CA. 2017. Operon mRNAs are organized into ORF-centric structures that predict translation efficiency. *eLife* **6**:e22037. doi:10.7554/eLife.22037
- Campo CD, Bartholomäus A, Fedyunin I, Ignatova Z. 2015. Secondary Structure across the Bacterial Transcriptome Reveals Versatile Roles in mRNA Regulation and Function. *PLOS Genet* **11**:e1005613. doi:10.1371/journal.pgen.1005613
- Davis MPA, van Dongen S, Abreu-Goodger C, Bartonicek N, Enright AJ. 2013. Kraken: A set of tools for quality control and analysis of high-throughput sequence data. *Methods, Diversity of the non-coding transcriptomes revealed by RNA-seq technologies* **63**:41–49. doi:10.1016/j.ymeth.2013.06.027
- de Smit MH, van Duin J. 2003. Translational standby sites: how ribosomes may deal with the rapid folding kinetics of mRNA. *J Mol Biol* **331**:737–743.
- de Smit MH, van Duin J. 1990. Secondary structure of the ribosome binding site determines translational efficiency: a quantitative analysis. *Proc Natl Acad Sci U S A* **87**:7668–7672. doi:10.1073/pnas.87.19.7668
- Duval M, Korepanov A, Fuchsbauer O, Fechter P, Haller A, Fabbretti A, Choulier L, Micura R, Klaholz BP, Romby P, Springer M, Marzi S. 2013. Escherichia coli ribosomal protein S1 unfolds structured mRNAs onto the ribosome for active translation initiation. *PLoS Biol* **11**:e1001731. doi:10.1371/journal.pbio.1001731
- Espah Borujeni A, Channarasappa AS, Salis HM. 2014. Translation rate is controlled by coupled trade-offs between site accessibility, selective RNA unfolding and sliding at upstream standby sites. *Nucleic Acids Res* **42**:2646–2659. doi:10.1093/nar/gkt1139

654 Espah Borujeni A, Salis HM. 2016a. Translation Initiation is Controlled by RNA Folding Kinetics via a  
 655 Ribosome Drafting Mechanism. *J Am Chem Soc* **138**:7016–7023. doi:10.1021/jacs.6b01453  
 656 Espah Borujeni A, Salis HM. 2016b. Translation Initiation is Controlled by RNA Folding Kinetics via a  
 657 Ribosome Drafting Mechanism. *J Am Chem Soc* **138**:7016–7023. doi:10.1021/jacs.6b01453  
 658 Evfratov SA, Osterman IA, Komarova ES, Pogorelskaya AM, Rubtsova MP, Zatsepin TS, Semashko TA,  
 659 Kostryukova ES, Mironov AA, Burnaev E, Krymova E, Gelfand MS, Govorun VM, Bogdanov AA,  
 660 Sergiev PV, Dontsova OA. 2017. Application of sorting and next generation sequencing to study  
 661 5'-UTR influence on translation efficiency in Escherichia coli. *Nucleic Acids Res* **45**:3487–3502.  
 662 doi:10.1093/nar/gkw1141  
 663 Gao R, Yu K, Nie J, Lian T, Jin J, Liljas A, Su X-D. 2016. Deep sequencing reveals global patterns of mRNA  
 664 recruitment during translation initiation. *Sci Rep* **6**:30170. doi:10.1038/srep30170  
 665 Goodman DB, Church GM, Kosuri S. 2013. Causes and effects of N-terminal codon bias in bacterial  
 666 genes. *Science* **342**:475–479. doi:10.1126/science.1241934  
 667 Gunderson JH, Sogin ML, Wollett G, Hollingdale M, de la Cruz VF, Waters AP, McCutchan TF. 1987.  
 668 Structurally distinct, stage-specific ribosomes occur in Plasmodium. *Science* **238**:933–937.  
 669 Hall MN, Gabay J, Débarbouillé M, Schwartz M. 1982. A role for mRNA secondary structure in the  
 670 control of translation initiation. *Nature* **295**:616–618. doi:10.1038/295616a0  
 671 Hockenberry AJ, Jewett MC, Amaral LAN, Wilke CO. 2018. Within-Gene Shine–Dalgarno Sequences Are  
 672 Not Selected for Function. *Mol Biol Evol* **35**:2487–2498. doi:10.1093/molbev/msy150  
 673 Hockenberry AJ, Stern AJ, Amaral LAN, Jewett MC. 2017. Diversity of translation initiation mechanisms  
 674 across bacterial species is driven by environmental conditions and growth demands. *Mol Biol*  
 675 *Evol.* doi:10.1093/molbev/msx310  
 676 Hui A, de Boer HA. 1987. Specialized ribosome system: preferential translation of a single mRNA  
 677 species by a subpopulation of mutated ribosomes in Escherichia coli. *Proc Natl Acad Sci U S A*  
 678 **84**:4762–4766.  
 679 Ingolia NT, Ghaemmaghami S, Newman JRS, Weissman JS. 2009. Genome-wide analysis in vivo of  
 680 translation with nucleotide resolution using ribosome profiling. *Science* **324**:218–223.  
 681 doi:10.1126/science.1168978  
 682 Ingolia NT, Lareau LF, Weissman JS. 2011. Ribosome Profiling of Mouse Embryonic Stem Cells Reveals  
 683 the Complexity and Dynamics of Mammalian Proteomes. *Cell* **147**:789–802.  
 684 doi:10.1016/j.cell.2011.10.002  
 685 Jacob WF, Santer M, Dahlberg AE. 1987. A single base change in the Shine-Dalgarno region of 16S rRNA  
 686 of Escherichia coli affects translation of many proteins. *Proc Natl Acad Sci U S A* **84**:4757–4761.  
 687 doi:10.1073/pnas.84.14.4757  
 688 Jiang H, Lei R, Ding S-W, Zhu S. 2014. Skewer: a fast and accurate adapter trimmer for next-generation  
 689 sequencing paired-end reads. *BMC Bioinformatics* **15**:182. doi:10.1186/1471-2105-15-182  
 690 Komarova AV, Tchufistova LS, Dreyfus M, Boni IV. 2005. AU-rich sequences within 5' untranslated  
 691 leaders enhance translation and stabilize mRNA in Escherichia coli. *J Bacteriol* **187**:1344–1349.  
 692 doi:10.1128/JB.187.4.1344-1349.2005  
 693 Kudla G, Murray AW, Tollervey D, Plotkin JB. 2009. Coding-sequence determinants of gene expression  
 694 in Escherichia coli. *Science* **324**:255–258. doi:10.1126/science.1170160  
 695 Kurylo CM, Parks MM, Juette MF, Zinshteyn B, Altman RB, Thibado JK, Vincent CT, Blanchard SC. 2018.  
 696 Endogenous rRNA Sequence Variation Can Regulate Stress Response Gene Expression and  
 697 Phenotype. *Cell Rep* **25**:236-248.e6. doi:10.1016/j.celrep.2018.08.093

698 Langmead B, Trapnell C, Pop M, Salzberg SL. 2009. Ultrafast and memory-efficient alignment of short  
 699 DNA sequences to the human genome. *Genome Biol* **10**:R25. doi:10.1186/gb-2009-10-3-r25  
 700 Lee K, Holland-Staley CA, Cunningham PR. 1996. Genetic analysis of the Shine-Dalgarno interaction:  
 701 selection of alternative functional mRNA-rRNA combinations. *RNA N Y N* **2**:1270–1285.  
 702 Lee Sooncheol, Liu B, Lee Soohyun, Huang S-X, Shen B, Qian S-B. 2012. Global mapping of translation  
 703 initiation sites in mammalian cells at single-nucleotide resolution. *Proc Natl Acad Sci U S A*  
 704 **109**:E2424–2432. doi:10.1073/pnas.1207846109  
 705 Li G-W. 2015. How do bacteria tune translation efficiency? *Curr Opin Microbiol*, Cell regulation **24**:66–  
 706 71. doi:10.1016/j.mib.2015.01.001  
 707 Li G-W, Burkhardt D, Gross C, Weissman JS. 2014. Quantifying absolute protein synthesis rates reveals  
 708 principles underlying allocation of cellular resources. *Cell* **157**:624–635.  
 709 doi:10.1016/j.cell.2014.02.033  
 710 Lodish HF. 1970. Secondary structure of bacteriophage f2 ribonucleic acid and the initiation of in vitro  
 711 protein biosynthesis. *J Mol Biol* **50**:689–702. doi:10.1016/0022-2836(70)90093-8  
 712 Majdalani N, Cuning C, Sledjeski D, Elliott T, Gottesman S. 1998. DsrA RNA regulates translation of  
 713 RpoS message by an anti-antisense mechanism, independent of its action as an antisilencer of  
 714 transcription. *Proc Natl Acad Sci U S A* **95**:12462–12467. doi:10.1073/pnas.95.21.12462  
 715 Mandal M, Breaker RR. 2004. Gene regulation by riboswitches. *Nat Rev Mol Cell Biol* **5**:451–463.  
 716 doi:10.1038/nrm1403  
 717 Meydan S, Marks J, Klepacki D, Sharma V, Baranov PV, Firth AE, Margus T, Kefi A, Vázquez-Laslop N,  
 718 Mankin AS. 2019. Retapamulin-Assisted Ribosome Profiling Reveals the Alternative Bacterial  
 719 Proteome. *Mol Cell* **74**:481–493.e6. doi:10.1016/j.molcel.2019.02.017  
 720 Mohammad F, Woolstenhulme CJ, Green R, Buskirk AR. 2016. Clarifying the Translational Pausing  
 721 Landscape in Bacteria by Ribosome Profiling. *Cell Rep* **14**:686–694.  
 722 doi:10.1016/j.celrep.2015.12.073  
 723 Moine H, Romby P, Springer M, Grunberg-Manago M, Ebel J-P, Ehresmann B, Ehresmann C. 1990.  
 724 Escherichia coli threonyl-tRNA synthetase and tRNAThr modulate the binding of the ribosome  
 725 to the translational initiation site of the ThrS mRNA. *J Mol Biol* **216**:299–310.  
 726 doi:10.1016/S0022-2836(05)80321-3  
 727 Mustoe AM, Busan S, Rice GM, Hajdin CE, Peterson BK, Ruda VM, Kubica N, Nutiu R, Baryza JL, Weeks  
 728 KM. 2018. Pervasive Regulatory Functions of mRNA Structure Revealed by High-Resolution  
 729 SHAPE Probing. *Cell* **173**:181–195.e18. doi:10.1016/j.cell.2018.02.034  
 730 Nakagawa S, Niimura Y, Miura K, Gojobori T. 2010. Dynamic evolution of translation initiation  
 731 mechanisms in prokaryotes. *Proc Natl Acad Sci* **107**:6382–6387. doi:10.1073/pnas.1002036107  
 732 Neumann H, Wang K, Davis L, Garcia-Alai M, Chin JW. 2010. Encoding multiple unnatural amino acids  
 733 via evolution of a quadruplet-decoding ribosome. *Nature* **464**:441–444.  
 734 doi:10.1038/nature08817  
 735 Orelle C, Carlson ED, Szal T, Florin T, Jewett MC, Mankin AS. 2015. Protein synthesis by ribosomes with  
 736 tethered subunits. *Nature* **524**:119–124. doi:10.1038/nature14862  
 737 Osterman IA, Evfratov SA, Sergiev PV, Dontsova OA. 2013. Comparison of mRNA features affecting  
 738 translation initiation and reinitiation. *Nucleic Acids Res* **41**:474–486. doi:10.1093/nar/gks989  
 739 Parks MM, Kurylo CM, Dass RA, Bojmar L, Lyden D, Vincent CT, Blanchard SC. 2018. Variant ribosomal  
 740 RNA alleles are conserved and exhibit tissue-specific expression. *Sci Adv* **4**:eaao0665.  
 741 doi:10.1126/sciadv.aao0665

742 Pfeiffer BD, Truman JW, Rubin GM. 2012. Using translational enhancers to increase transgene  
 743 expression in *Drosophila*. *Proc Natl Acad Sci* **109**:6626–6631. doi:10.1073/pnas.1204520109  
 744 Qu X, Lancaster L, Noller HF, Bustamante C, Tinoco I. 2012. Ribosomal protein S1 unwinds double-  
 745 stranded RNA in multiple steps. *Proc Natl Acad Sci U S A* **109**:14458–14463.  
 746 doi:10.1073/pnas.1208950109  
 747 Rackham O, Chin JW. 2005. A network of orthogonal ribosome x mRNA pairs. *Nat Chem Biol* **1**:159–  
 748 166. doi:10.1038/nchembio719  
 749 Ranjan A, Hasnain SE. 1995. Influence of codon usage and translational initiation codon context in the  
 750 AcNPV-based expression system: computer analysis using homologous and heterologous genes.  
 751 *Virus Genes* **9**:149–153.  
 752 Rex G, Surin B, Besse G, Schneppe B, McCarthy JE. 1994. The mechanism of translational coupling in  
 753 *Escherichia coli*. Higher order structure in the atpHA mRNA acts as a conformational switch  
 754 regulating the access of de novo initiating ribosomes. *J Biol Chem* **269**:18118–18127.  
 755 Salis HM, Mirsky EA, Voigt CA. 2009. Automated Design of Synthetic Ribosome Binding Sites to  
 756 Precisely Control Protein Expression. *Nat Biotechnol* **27**:946–950. doi:10.1038/nbt.1568  
 757 Sano K-I, Maeda K, Oki M, Maéda Y. 2002. Enhancement of protein expression in insect cells by a  
 758 lobster tropomyosin cDNA leader sequence. *FEBS Lett* **532**:143–146. doi:10.1016/s0014-  
 759 5793(02)03659-1  
 760 Schrader JM, Zhou B, Li G-W, Lasker K, Childers WS, Williams B, Long T, Crosson S, McAdams HH,  
 761 Weissman JS, Shapiro L. 2014. The Coding and Noncoding Architecture of the *Caulobacter*  
 762 *crescentus* Genome. *PLOS Genet* **10**:e1004463. doi:10.1371/journal.pgen.1004463  
 763 Shine J, Dalgarno L. 1974. The 3'-Terminal Sequence of *Escherichia coli* 16S Ribosomal RNA:  
 764 Complementarity to Nonsense Triplets and Ribosome Binding Sites. *Proc Natl Acad Sci U S A*  
 765 **71**:1342–1346.  
 766 Song W, Joo M, Yeom J-H, Shin E, Lee M, Choi H-K, Hwang J, Kim Y-I, Seo R, Lee JE, Moore CJ, Kim Y-H,  
 767 Eyun S, Hahn Y, Bae J, Lee K. 2019. Divergent rRNAs as regulators of gene expression at the  
 768 ribosome level. *Nat Microbiol* **4**:515. doi:10.1038/s41564-018-0341-1  
 769 Spahn CM, Beckmann R, Eswar N, Penczek PA, Sali A, Blobel G, Frank J. 2001. Structure of the 80S  
 770 ribosome from *Saccharomyces cerevisiae*--tRNA-ribosome and subunit-subunit interactions.  
 771 *Cell* **107**:373–386.  
 772 Steitz JA, Jakes K. 1975. How ribosomes select initiator regions in mRNA: base pair formation between  
 773 the 3' terminus of 16S rRNA and the mRNA during initiation of protein synthesis in *Escherichia*  
 774 *coli*. *Proc Natl Acad Sci U S A* **72**:4734–4738.  
 775 Storz G, Opdyke JA, Zhang A. 2004. Controlling mRNA stability and translation with small, noncoding  
 776 RNAs. *Curr Opin Microbiol* **7**:140–144. doi:10.1016/j.mib.2004.02.015  
 777 Suzuki T, Ito M, Ezure T, Kobayashi S, Shikata M, Tanimizu K, Nishimura O. 2006. Performance of  
 778 expression vector, pTD1, in insect cell-free translation system. *J Biosci Bioeng* **102**:69–71.  
 779 doi:10.1263/jbb.102.69  
 780 Weaver J, Mohammad F, Buskirk AR, Storz G. 2019. Identifying Small Proteins by Ribosome Profiling  
 781 with Stalled Initiation Complexes. *mBio* **10**:e02819-18. doi:10.1128/mBio.02819-18  
 782 Winkler W, Nahvi A, Breaker RR. 2002. Thiamine derivatives bind messenger RNAs directly to regulate  
 783 bacterial gene expression. *Nature* **419**:952–956. doi:10.1038/nature01145



784 Woolstenhulme CJ, Guydosh NR, Green R, Buskirk AR. 2015. High-precision analysis of translational  
785 pausing by ribosome profiling in bacteria lacking EFP. *Cell Rep* **11**:13–21.  
786 doi:10.1016/j.celrep.2015.03.014  
787 Wu X, Bartel DP. 2017. kpLogo: positional k-mer analysis reveals hidden specificity in biological  
788 sequences. *Nucleic Acids Res* **45**:W534–W538. doi:10.1093/nar/gkx323  
789 Youngman EM, Brunelle JL, Kochaniak AB, Green R. 2004. The active site of the ribosome is composed  
790 of two layers of conserved nucleotides with distinct roles in peptide bond formation and  
791 peptide release. *Cell* **117**:589–599.  
792 Youngman EM, Green R. 2005. Affinity purification of in vivo-assembled ribosomes for in vitro  
793 biochemical analysis. *Methods San Diego Calif* **36**:305–312. doi:10.1016/j.ymeth.2005.04.007  
794  
795  
796

## Figure Captions

**Figure 1.** Capturing the role of SD motifs by MS2RP. (A) ASD mutations at the 3'-end of 16S rRNA are highlighted in color. (B) Schematic of MS2RP: polysomes are collapsed to monosomes by RNase T1 digestion, MS2-tagged monosomes are pulled down with the MS2 coat-protein, and mRNA is fully digested to yield ribosome footprints that are subjected to deep sequencing. (C) RT-PCR of 16S rRNA from cell lysates (L) and the eluate (E) from the MS2 coat-protein column. (D) Scatter plot of ribosome occupancy (RO), the ratio of ribosome profiling to RNA-seq reads, from MS2RP of O-ribosomes vs. C-ribosomes. The red line indicates a 10-fold enrichment and the Pearson correlation is given. (E) Ribosome footprints (in reads per million mapped reads) from MS2RP of O-ribosomes and C-ribosomes on the *hemA* gene. The sequence upstream of the start codon is predicted to pair with the ASD of O-ribosomes.

**Figure 1-figure supplement 1.** (A) Growth of *E. coli* MG1655 cells expressing MS2-tagged 16S rRNA from a promoter induced by IPTG. (B) Polysome profiles after 25 min of induction of MS2-tagged ribosomes. (C) RNA-seq analysis of rRNA affinity-purified by the MS2 protein in the absence of nuclease treatment. This procedure should capture all MS2-containing rRNA including processing intermediates. The 16S rRNA ends at 1895 in the mutants as well as in the wild-type, suggesting that there are not gross defects in the processing of the 3'-end of 16S rRNA. (D) position of MS2-tagged ribosomes across the sucrose gradient in cell lysates (L) and light (P1) and heavy (P2) polysomes as detected by RT-PCR of the 16S rRNA.

**Figure 1-figure supplement 2.** Enhanced translation of genes with ribosome-binding sites complementary to ASD-mutant ribosomes. (A,B) Ribosome density (in reads per million mapped reads) from MS2RP of O- and C-ribosomes on the *rbsK* and *mreB* genes. (C,D) Ribosome density from MS2RP of S- and C-ribosomes on the *sapA* and *rsmH* genes.

**Figure 2.** MS2RP reveals that SD motifs enhance translation genome-wide. Ribosome occupancy (RO) is the ratio of ribosome profiling to RNA-seq reads per gene.  $\log_{10}RO$  values are plotted against the SD strength ( $-\Delta G$  of pairing to the wild-type ASD) for each gene with MS2RP data for C-ribosomes (A) and A-ribosomes (B). (C) Scatter plot of  $\Delta \log RO$  (C-ribosomes minus A-ribosomes) and  $-\Delta G$  where  $r$  values indicate Pearson correlations.

**Figure 2-figure supplement 1.** MS2RP reveals that SD motifs enhance ribosome occupancy. Scatter plots of  $\log_{10}RO$  and SD strength ( $-\Delta G$  of pairing to the wild-type ASD) for O-ribosomes (A) and S-ribosomes (B). (B,D) Scatter plot of  $\Delta \log RO$  (C-ribosomes minus O- or S-ribosomes) and  $-\Delta G$  where the  $r$  values indicate Pearson correlations.

**Figure 2-figure supplement 2.** Genes translated better by wild-type ribosomes than by ASD mutants have sequences between -15 and -6 nt upstream of the start codon with high affinity to the ASD. (A) Genes with the top 15% of  $\Delta \log RO$  values are translated better by the wild-type ribosomes than by ASD mutants and are therefore SD dependent. In contrast, those in the bottom 15% are SD independent. (B) We computed the free energy of base pairing to the wild-type ASD for a tiled set of nine 10 nt windows. (C) Histograms showing the window with the strongest affinity to the wild-type ASD for each

mRNA in the set of SD-dependent (left) and SD-independent genes (right) for each of the three ASD mutant datasets. (D) Plots of  $\Delta G$  of pairing to the WT ASD for individual genes; the thick line indicates the mean of the group. Taken together, these results confirm that we captured the role of SD motifs by MS2RP and justify the use of pairing energies from the -15 to -6 window in this report.

**Figure 3.** Loss of SD-ASD pairing has little effect on start codon selection. (A,B) Ribosome footprints on *lpp* and *gmk* from MS2RP data obtained with and without retapamulin, an antibiotic that traps ribosomes at start codons. Annotated AUGs are indicated by a red bar, non-annotated AUGs are indicated by blue bars. (C, D) Average ribosome protected fragments (RPFs) at annotated AUGs and non-annotated AUGs (where AUG starts at 1). (E) Average RPFs at the start codon of genes whose ribosome-binding sites have little or no affinity to all three mutant ASD sequences.

**Figure 3-figure supplement 1.** Ribosome density at annotated start sites does not depend on SD-ASD base pairing. Average ribosome footprints aligned at annotated start sites that have high affinity to the wild-type (A), O-ribosomes (B), and S-ribosomes (C). There were not enough start sites with high affinity to the A-ribosomes for a similar analysis.

**Figure 4.** The effects of SD-ASD pairing on initiation at non-canonical sites. (A) Evaluation of initiation score, IS. (B) Initiation scores on non-annotated AUG triplets. For C-ribosomes, the fraction with IS > 1.5 is colored black. (C) Initiation scores for C- and A-ribosomes for the set of sites with IS > 1.5 for C-ribosomes (High, colored black in Figure 4B) and those with IS < 1.5 (Low). (D,E) IS values for all four ribosome types on the subset of sites with high affinity for the ASD of the S-ribosome (CCUCC). Average RPFs at the AUG triplets with high IS scores (F) or low IS scores (G) from the S-ribosome data.

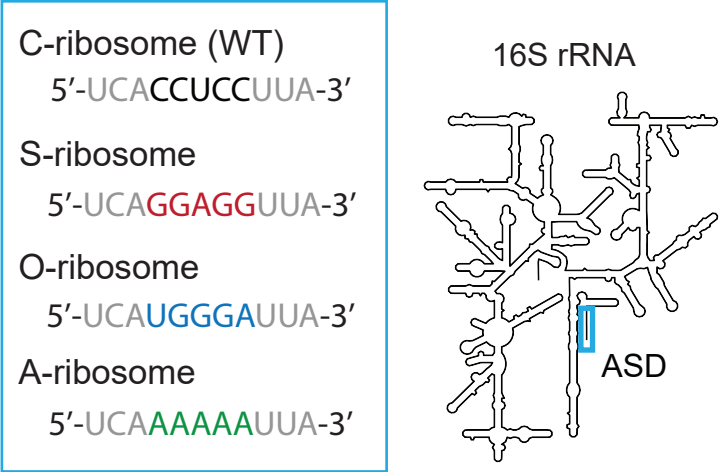
**Figure 4-figure supplement 1.** The effects of SD-ASD pairing on initiation at non-canonical sites. (A) Initiation score (IS) values for all four ribosome types on the subset of non-annotated AUGs in the transcriptome with high affinity for wild-type ASD. (B,C) Average RPFs at AUGs with high IS scores or low IS scores at sites with high affinity for the wild-type ASD (black and grey in panel A, respectively).

**Figure 5.** A-rich sequences as a signal for start codon selection. (A) Probability logo of the region surrounding annotated AUGs with low affinity to the wild-type ASD sequence ( $\Delta G > 0$ ) as compared with all non-annotated AUGs in the transcriptome. Enriched nucleotides are shown above the axis and depleted nucleotides below the axis. The height of the letter represents the binomial P-value. (B) Design of the reporter assay. The reporter plasmid encodes mCherry with a strong ribosome binding site (RBS) and separately GFP downstream of a region containing a start site of interest (30 nt upstream of AUG and 42 nt downstream). (C) Initiation sites used in the reporter assay; the number indicates the genomic position of AUG. In the T- and C-mutants, the A's upstream of AUG (highlighted in green) were substituted by T or C. (D) Results of the reporter assay. Each dot is the median of GFP/mCherry from an independent run of flow cytometry. The bar graph indicates the mean and SD from 4 independent tests. NoGFP (a plasmid that encodes mCherry but not GFP) serves as a control showing the baseline signal from cellular autofluorescence; the other data are normalized to this ratio. (E) Median (solid line) and interquartile range (shaded) of mRNA structure in SHAPE-MaPseq data for 365 annotated start sites (red) and 7,310 non-annotated AUGs within coding sequences (blue).

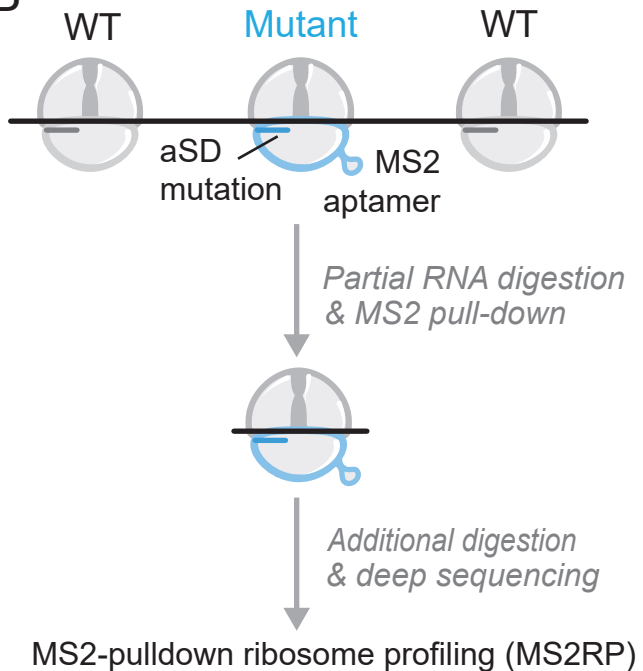
885 **Figure 5-figure supplement 1.** A-rich sequences near start codons throughout the Bacterial kingdom.  
886 Probability logo showing sequences enriched (above the x-axis) in annotated AUGs compared with  
887 non-annotated AUGs in ORFs.  
888  
889

Figure 1

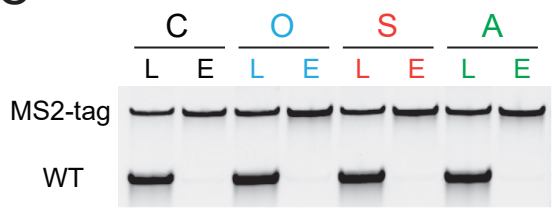
A



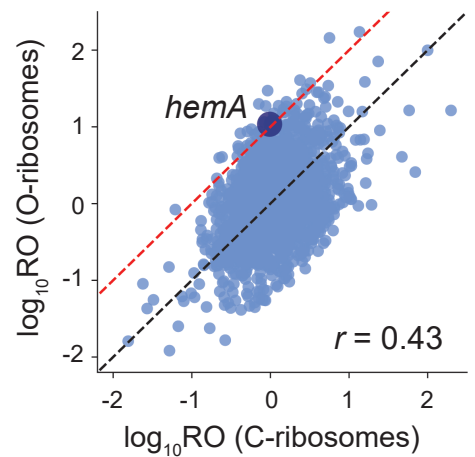
B



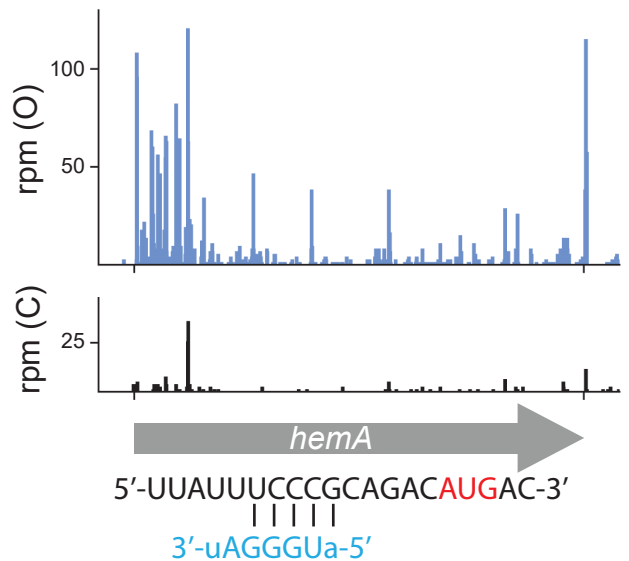
C

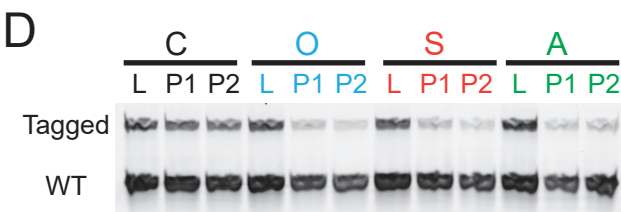
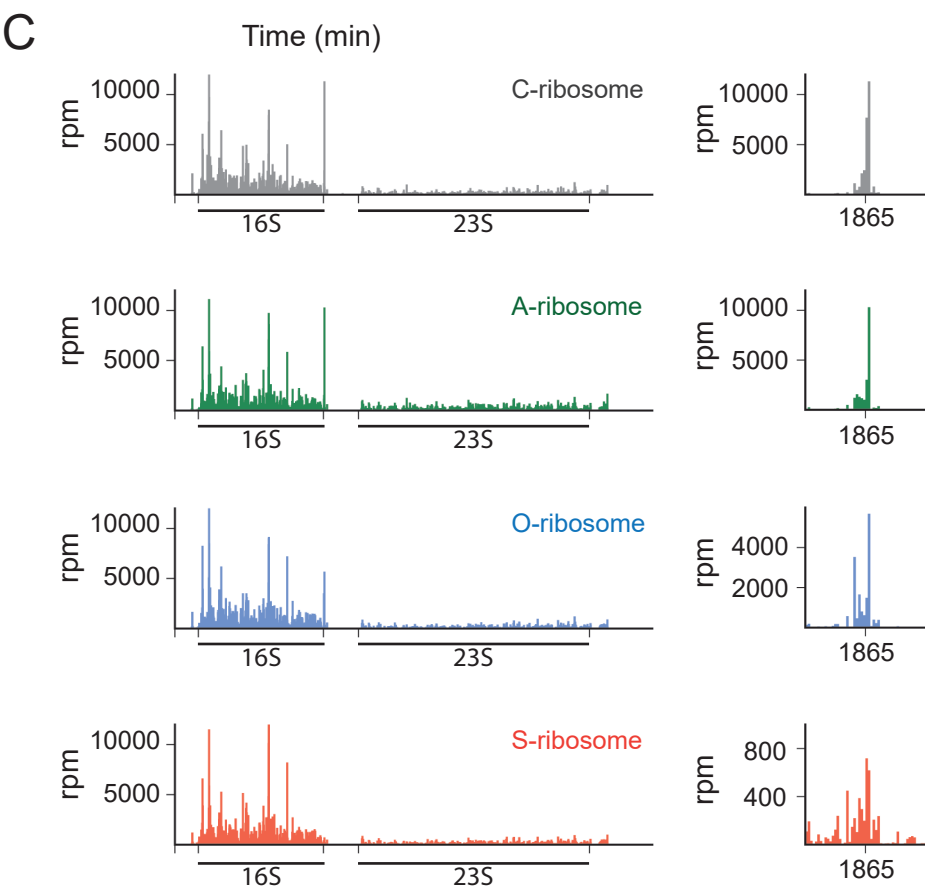
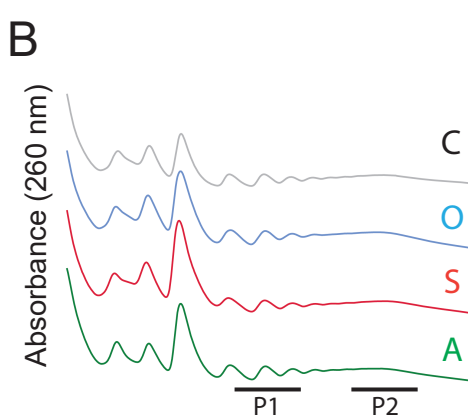
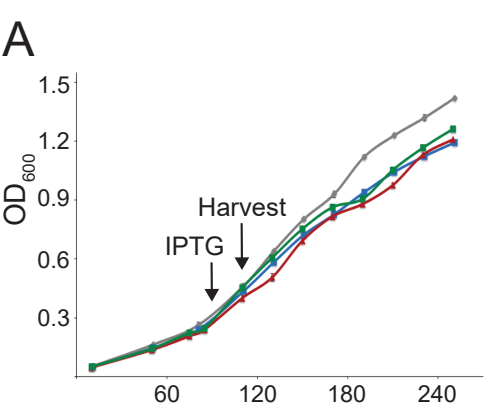


D



E





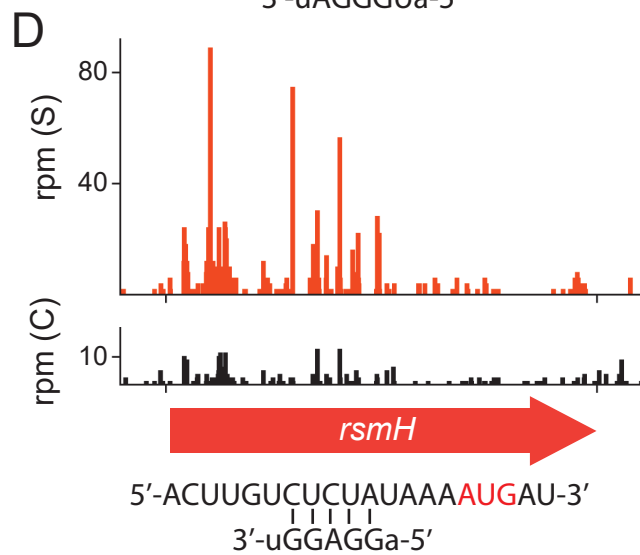
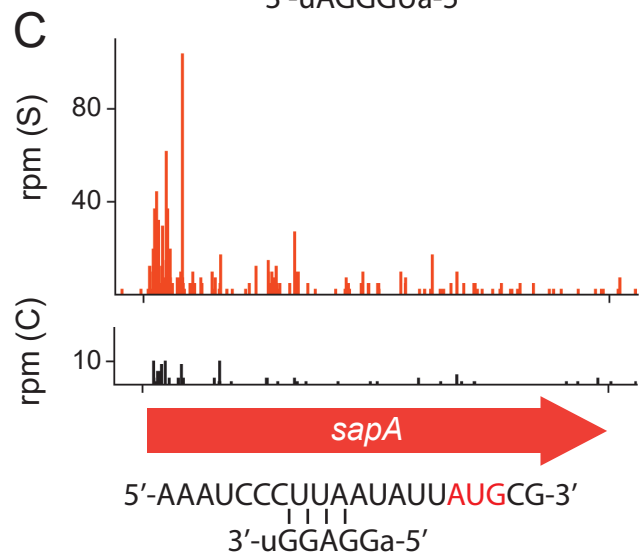
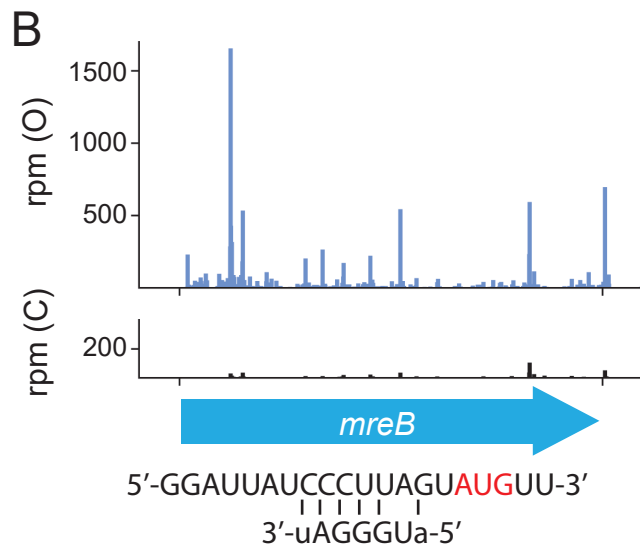
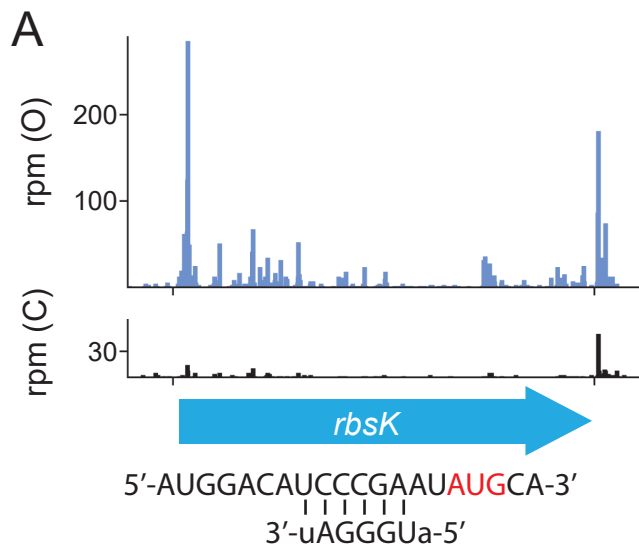
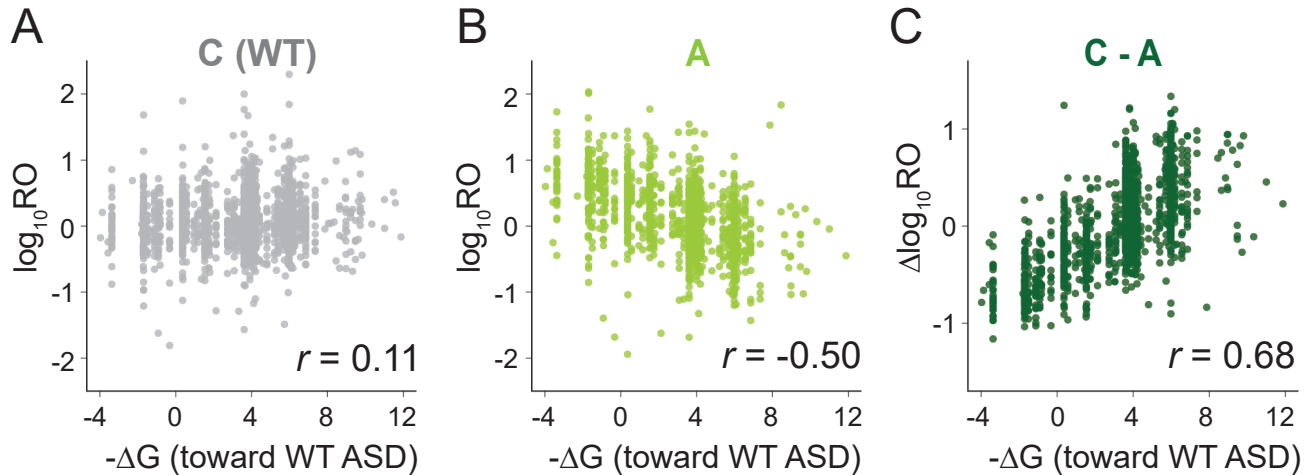
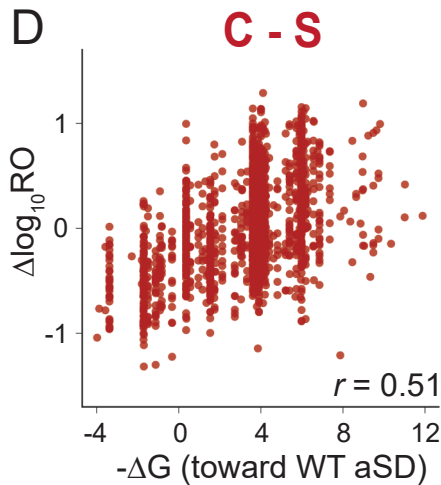
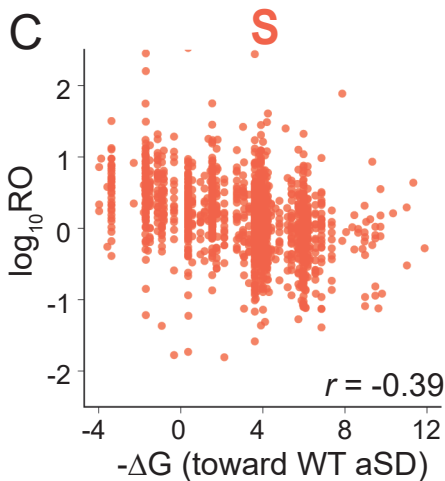
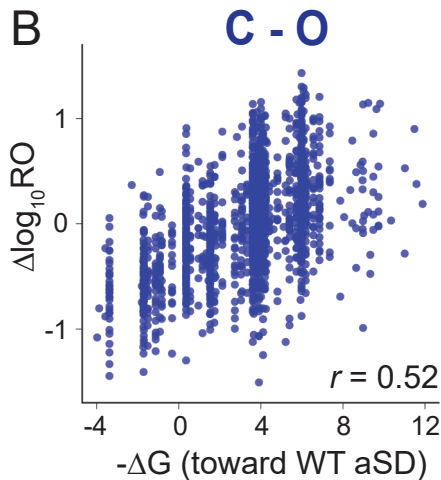
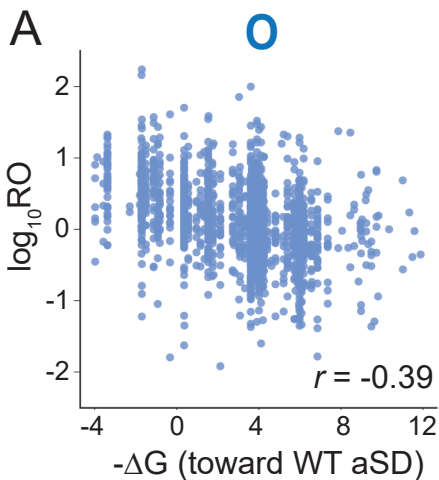


Figure 2







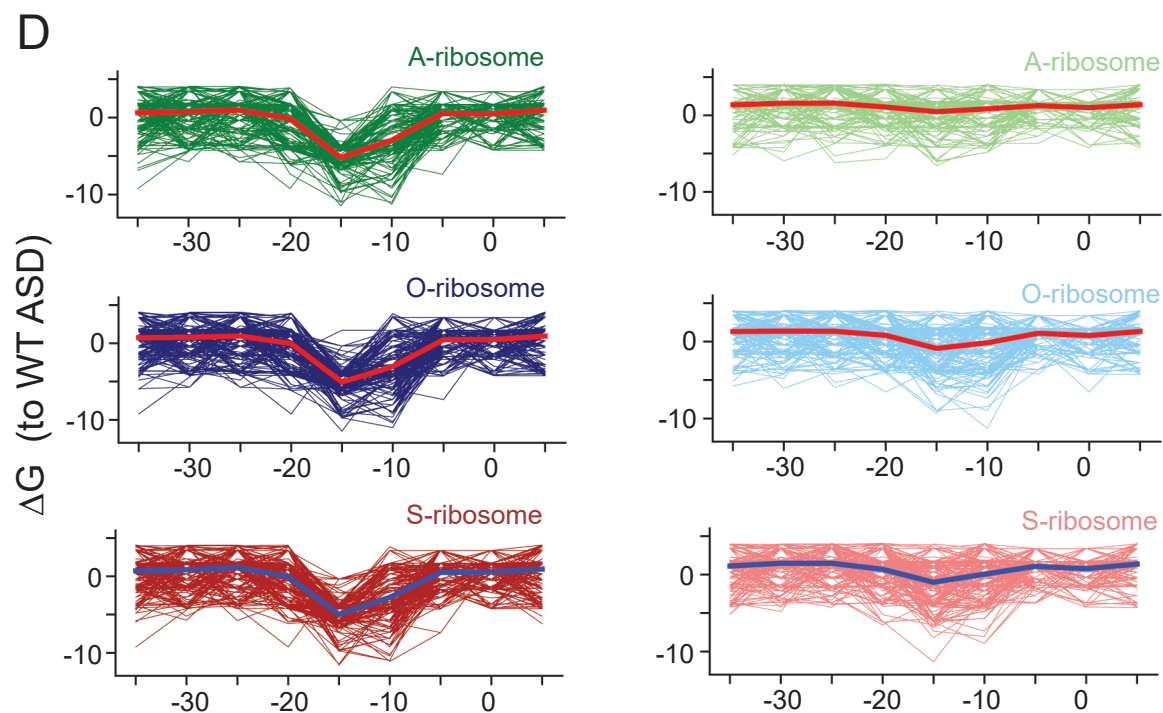
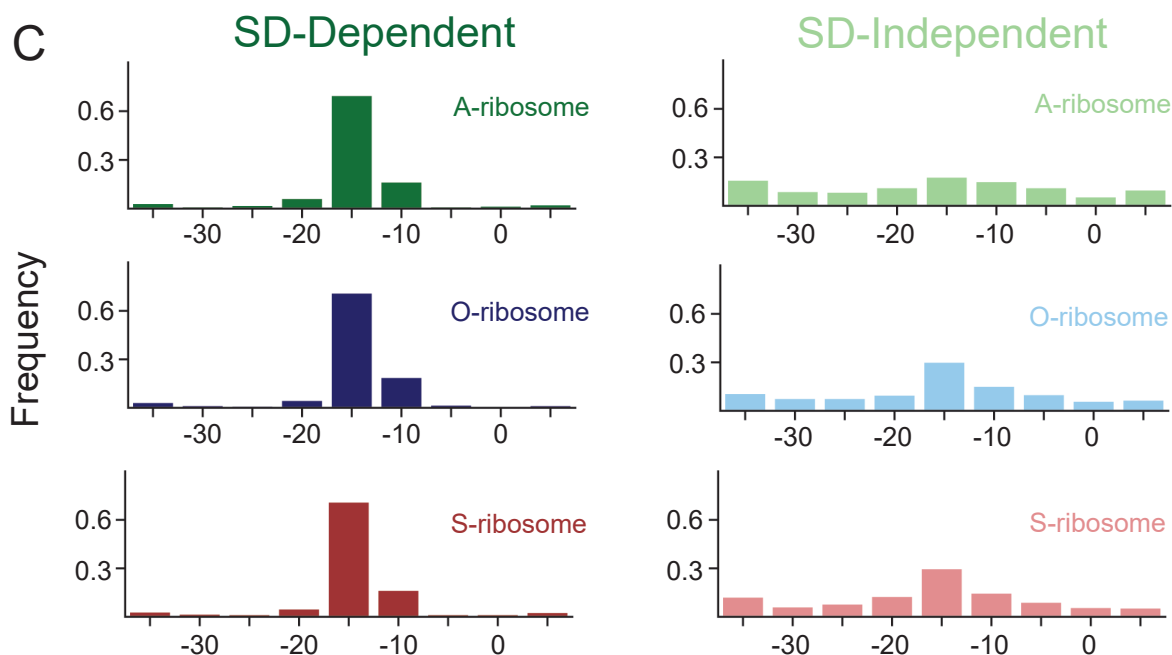
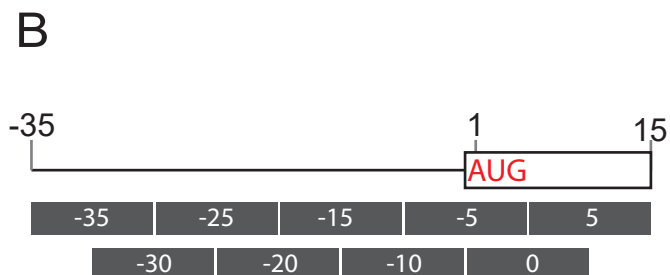
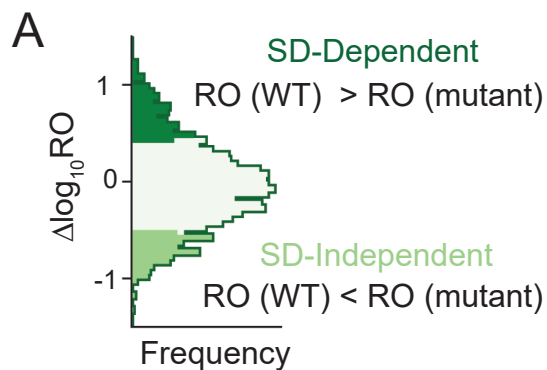
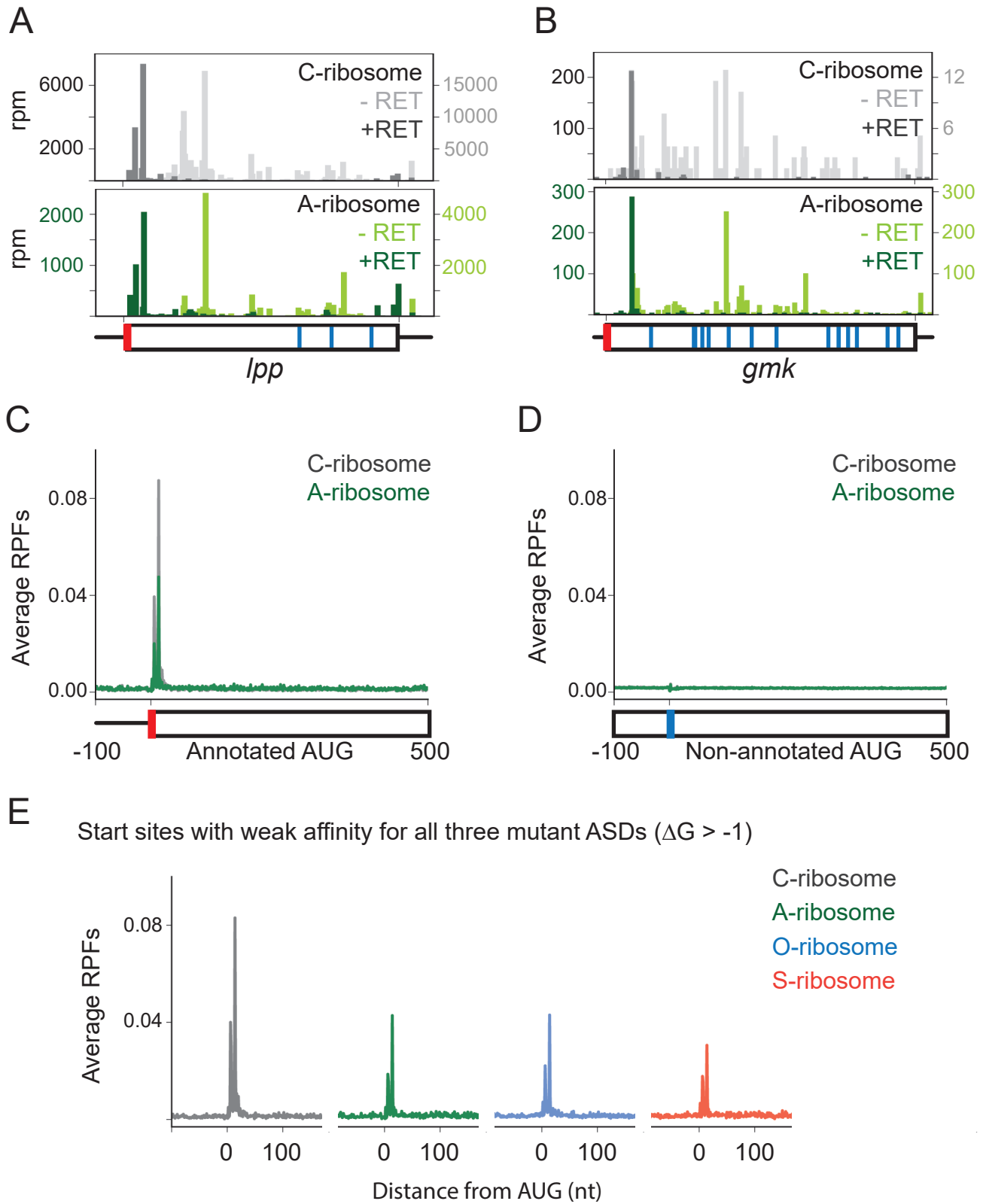
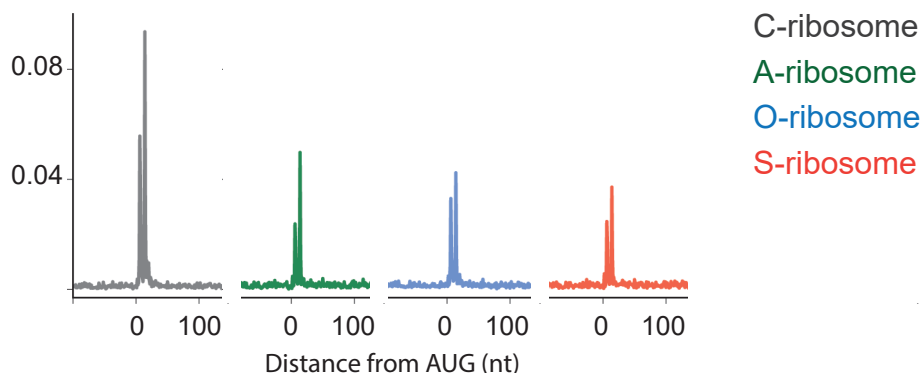


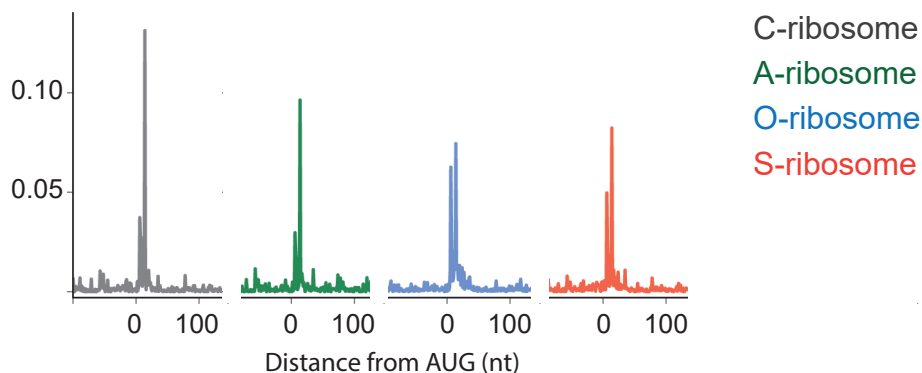
Figure 3



A

Start sites with strong affinity toward WT ( $\Delta G$  toward CCUCC < -4) N~700

B

Start sites with strong affinity toward O-ribosome ( $\Delta G$  toward AGGGU < -4) N~90

C

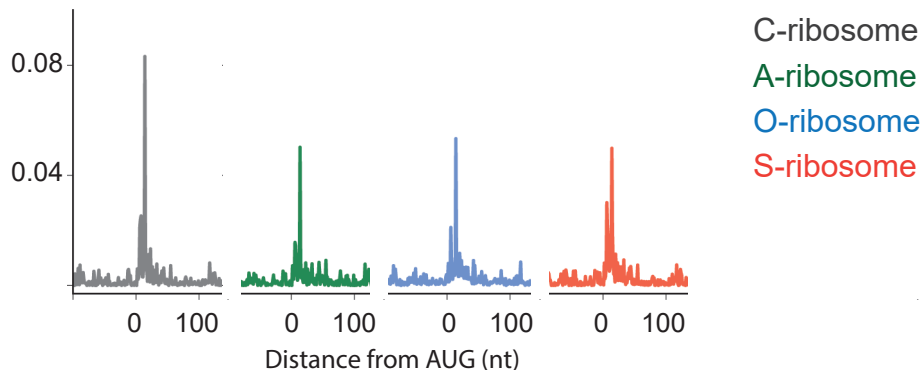
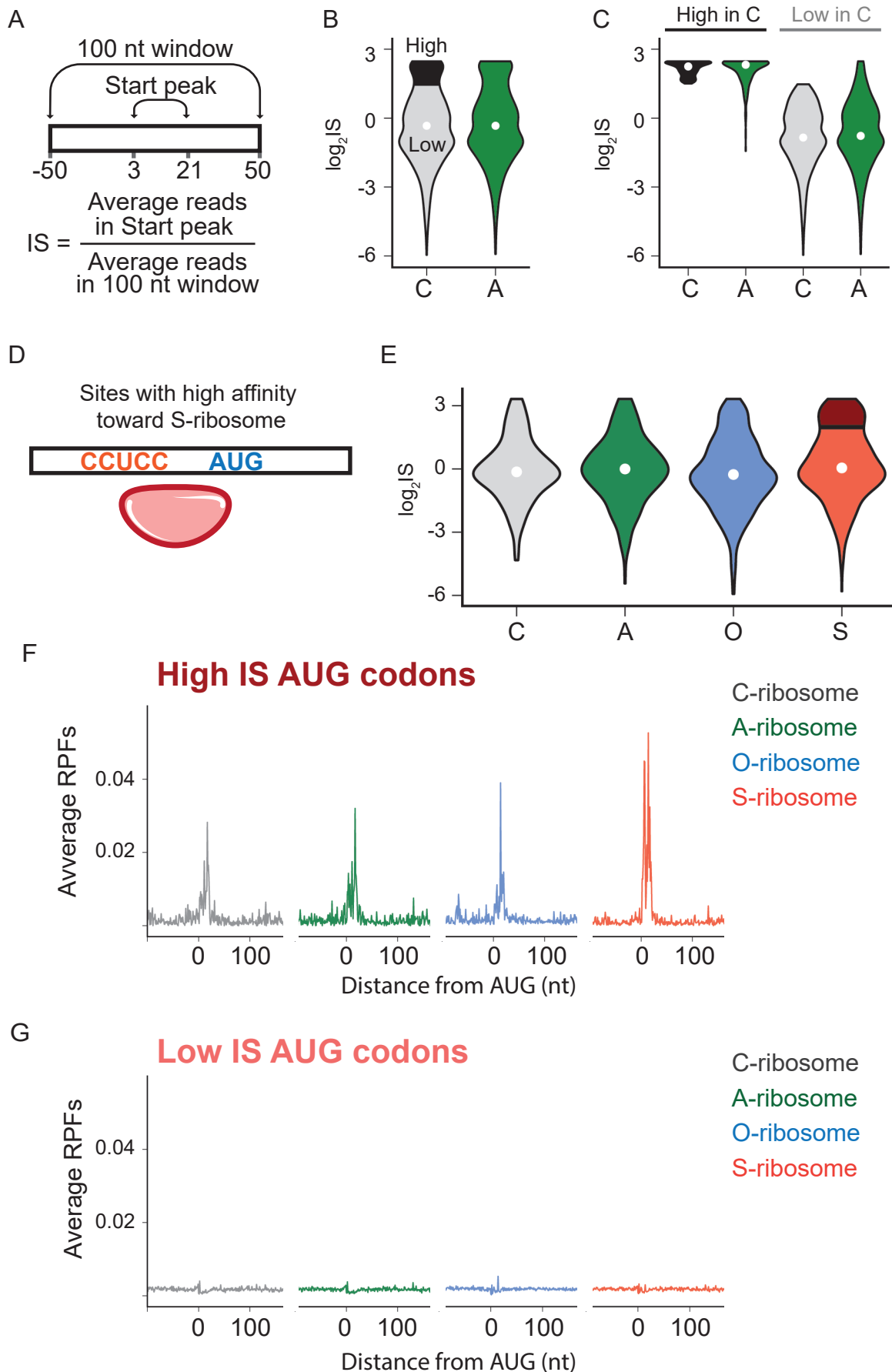
Start sites with strong affinity toward S-ribosome ( $\Delta G$  toward GGAGG < -4) N~90

Figure 4



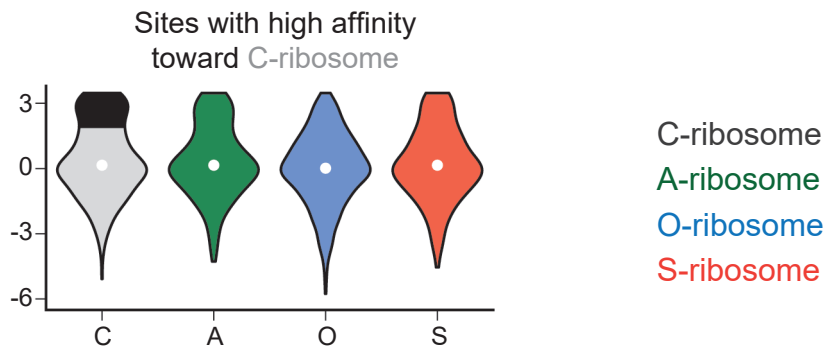
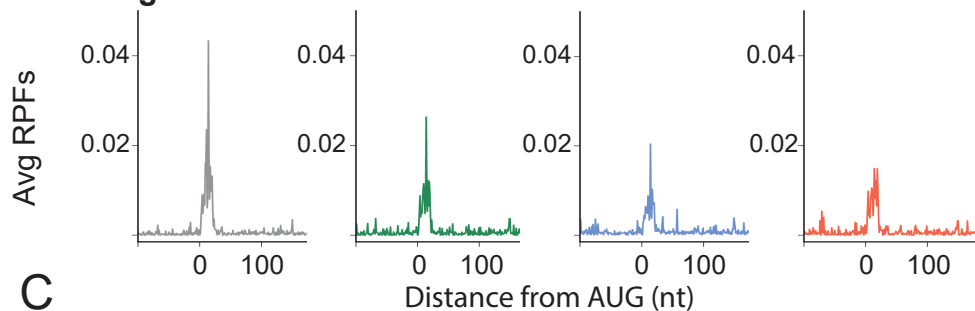
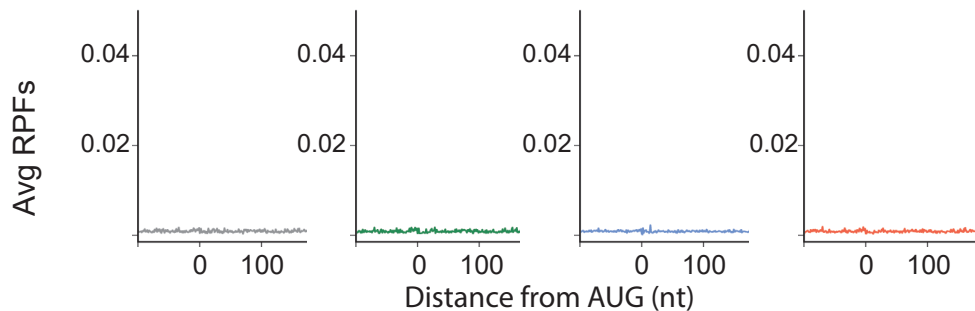
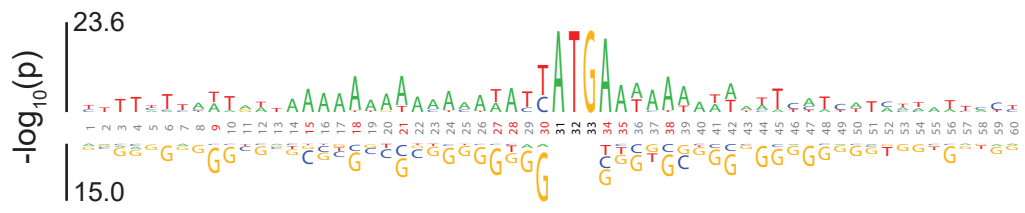
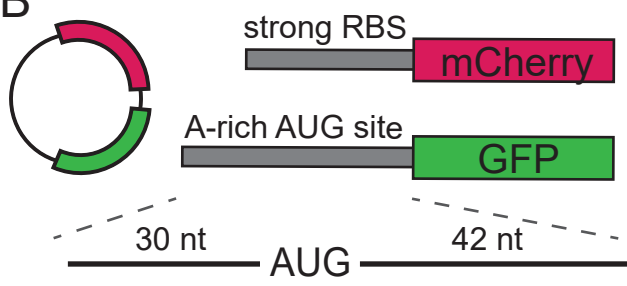
**A****B****High IS AUGs****C****Low IS AUGs**

Figure 5

A



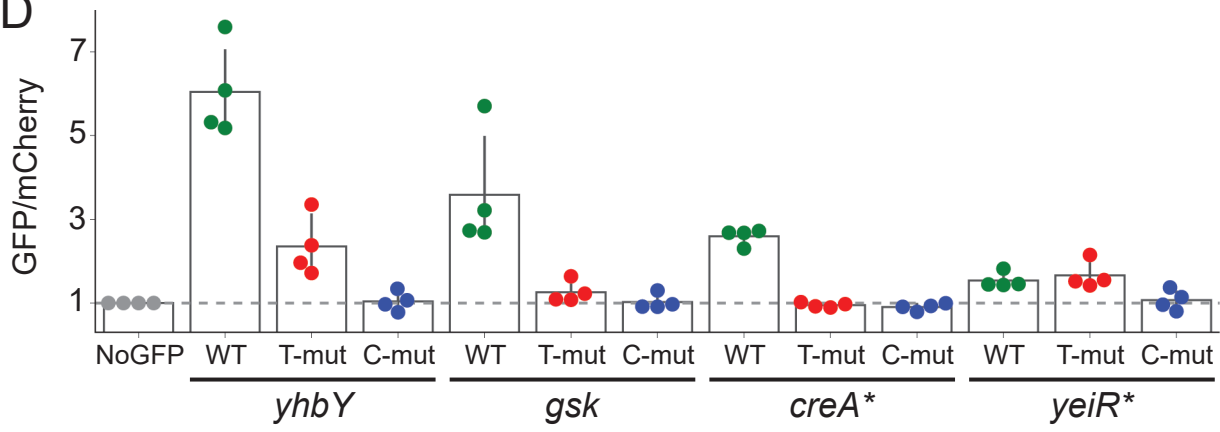
B



C

*yhby* (3325812)  
CAACGTAAGCAAAAAATACGATGAATCTG  
*gsk* (499349)  
AACCACCCGTAAAAACAACCATGAAATTT  
-----  
*creA\** (4633698)  
TGATGATCCCGATGTGAAAAATGTCACCT  
*yeiR\** (2265943)  
CATAAAGATCCCCAACGAAAAATGGGCGGT

D



E

